FIBER FABRY-PEROT INTERFEROMETER (FFPI) SENSOR

USING VERTICAL CAVITY SURFACE EMITTING LASER (VCSEL)

A Dissertation

by

KYUNG-WOO LEE

Submitted to the Office of Graduate Studies of
Texas A&M University
in partial fulfillment of the requirements for the degree of

DOCTOR OF PHILOSOPHY

August 2005

Major Subject: Electrical Engineering

FIBER FABRY-PEROT INTERFEROMETER (FFPI) SENSOR

USING VERTICAL CAVITY SURFACE EMITTING LASER (VCSEL)

A Dissertation

by

KYUNG-WOO LEE

Submitted to the Office of Graduate Studies of
Texas A&M University
in partial fulfillment of the requirements for the degree of

DOCTOR OF PHILOSOPHY

Approved by:

Chair of committee,	Henry F. Taylor
Committee members,	Chin B. Su
	Ohannes Eknoyan
	Alvin T. Yeh
Head of Department,	Chanan Singh

August 2005

Major Subject: Electrical Engineering

ABSTRACT

Fiber Fabry-Perot Interferometer (FFPI) Sensor Using

Vertical Cavity Surface Emitting Laser (VCSEL). (August 2005)

Kyung-Woo Lee, B.S., Hanyang University;

M.S., Texas A&M University

Chair of Advisory Committee: Dr. Henry F. Taylor

This research represents the first effort to apply vertical cavity surface emitting lasers (VCSELs) to the monitoring of interferometric fiber optic sensors. Modulation of the drive current causes thermal tuning of the laser light frequency. Reflection of this frequency-modulated light from a fiber Fabry-Perot interferometer (FFPI) sensor produces fringe patterns which can be used to measure the optical path difference of the sensor. Spectral characteristics were measured for 850nm VCSELs to determine the combination of dc bias current, modulation current amplitude and modulation frequency for which single mode VCSEL operation and regular fringe patterns are achieved. The response characteristics of FFPI sensors were determined experimentally for square, triangular, saw-tooth waveforms at frequencies from 10kHz to 100kHz. The dependence of VCSEL frequency on the dc bias current was determined from spectral measurements to be ~165GHz/mA. An independent measurement of this quantity based on counting fringes from the FFPI sensor as the laser modulated was in good agreement with this value. The effect of optical feedback into the laser was also studied. By observing the fringe shift as the FFPI sensor was heated, a fractional change in optical length with

temperature of 6.95 X 10^{-6}/°C was determined in good agreement with previous measurements on a 1300nm single mode fiber. The performance of 850nm VCSEL/FFPI systems was compared with their counterparts using 1300nm distributed feedback (DFB) lasers. The results of these experiments show that the 850nm VCSEL/FFPI combination gives regular fringe patterns at much lower bias current and modulating current amplitudes than their 1300nm DFB/FFPI counterparts.

ACKNOWLEDGMENTS

I would like to express my very sincere gratitude to Dr. Henry, F. Taylor, the chair of my advisory committee, for his guidance, support, and helpful advice during my research work. Not only his profound knowledge but also his generosity and patience deserve my great respect and appreciation. I would also like to express my appreciation to Dr. Chin B. Su, Dr. Ohannes Eknoyan, and Dr. Alvin T. Yeh for their advice as my committee members. I also gratefully offer special thanks to Dr. Bob Biard for his advice on the experiments with the VCSELs. I would also like to thank Mr. Robert Atkins for his help on fiber coating.

I would like to thank all the current students in our laboratory, especially Mr. Taehan Bae, for his helpful advice and encouragement in making FFPI sensors. I also would like to thank the former students in our laboratory, especially Mr. Jongseo Lee and Mr. Seongmin Yim, for their support and advice. I would like to thank current students in solid state lab, especially Mr. Ryounghan Kim, Mr. Yongwook Sin, and Mr. Sungkyu Seo, for their advice.

Special thanks to my parents, Dr. Changkoo Lee and Mrs. Kyusoon Kim, for their unfading love and sacrifice. The same thanks my brother, Mr. Sungwoo Lee and his wife Yeonju Yoon, for support during my studies.

TABLE OF CONTENTS

Page

CHAPTER Page

LIST OF FIGURES

Page

Page

Page

Page

Page

LIST OF TABLES

Page

CHAPTER I

INTRODUCTION

I. A Overview

Fiber optic sensor technology has been driven by the need for components to support the optoelectronic and fiber optic communication industry. The falling prices and quality improvements in these components have made it possible for fiber optic sensors to displace traditional sensors for acceleration, chemical measurement, electric field measurement, humidity, pressure, rotation, temperature, acoustics, vibration, strain, and viscosity [1]. Inherent advantageous features of the fiber sensor vs. traditional sensors technologies include: high sensitivity, long life at elevated temperatures, safety in the presence of volatile substances, immunity to electromagnetic interference, light weight, and mechanically flexibility and ruggedness. The sensors are also amenable to multiplexing [2].

Fiber optic sensors are often grouped as extrinsic or hybrid fiber and intrinsic. Extrinsic fiber optic sensors consist of optical fibers that lead up to and out of a black box which modulates the light beam passing through it in response to an environmental effect. The intrinsic fiber sensor relies on the light beam propagating through the optical fiber being modulated by the environmental effect through environmentally induced optical path length changes[2].

Journal model is *Journal of Lightwave Technology.*

One of the areas of greatest interest has been in the development of high performance interferometric fiber optic sensors with Michelson, Mach-Zehnder, Sagnac, and Fabry-Perot configurations.

Fig. 1 shows the basic element of a Mach-Zehnder interferometer. A light beam is split into two paths, one light beam is isolated from environmental effects as a reference arm and the other light beam is affected by the environmental perturbation of interest known as a measurand. A change in the optical path difference between the two light beams is induced by the measurand. If a Mach-Zehnder interferometer is arranged so that its reference and signal legs differ in length by L1-L2, then the net phase difference between the two light beams is

$$\Delta\phi = \frac{2\pi n(L_1 - L_2)}{\lambda} \tag{1}$$

where n is the refractive index of the fiber and λ is wavelength of the light source, where L_1 and L_2 are the lengths of the sensing arm and reference arm respectively.

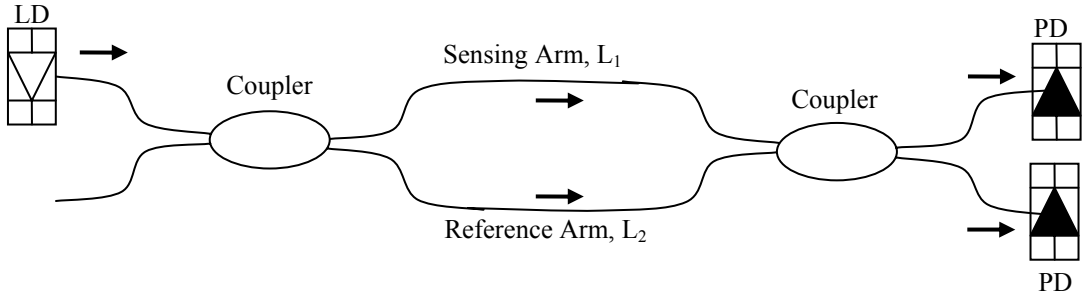

Fig. 1 Fiber optic Mach-Zehnder interferometer.

Fig.2 shows a fiber optic Michelson interferometer. Like the Mach-Zehnder, the measurand induces an optical path difference between the sensing arm and the reference arm in the Michelson interferometer. Where Mach-Zehnder interferometers need two couplers and two photodetectors, the Michelson interferometer only requires one coupler and one photodetector. Mach-Zehnder interferometers have the advantage of no back reflection to the light source.

In the Michelson interferometer, a beam from the light source is divided into two paths and light is reflected back to the coupler by two mirrors. The photodetector collects reflected light from one arm of the coupler. The phase shifts between the two arms is

$$\Delta\phi = \frac{4\pi n(L_1 - L_2)}{\lambda} \tag{2}$$

where L_1 and L_2 are the lengths of the sensing arm and reference arm respectively.

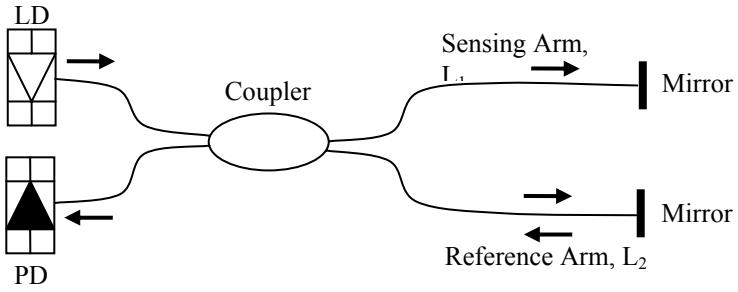

Fig. 2 Fiber optic Michelson interferometer.

The fiber Sagnac interferometer, as shown in Fig. 3, consists of a multiple winding fiber coil and a 3 dB coupler. The light travels in opposite directions in the fiber

coil and recombines at the coupler. Rotation of the interferometer about axis perpendicular to the plane of the coil causes a phase shift given by

$$\Delta\phi = \frac{4\pi LR}{\lambda c}\Omega \tag{3}$$

where R is the radius of the fiber coil, L is the fiber length of the coil, λ is the wavelength of the injected light, c is the free space speed of light, and Ω is the rotation rate of the platform on which the interferometer is mounted. This phase shift is due to difference in propagation time delays between the two counter propagating beams; this is known as the Sagnac effect. This is the basis of the fiber gyroscope [3].

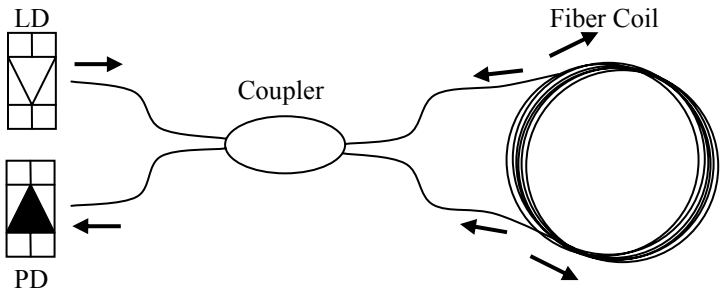

Fig. 3 Fiber optic Sagnac interferometer.

Another implementation of the interferometric sensor is the Fabry-Perot interferometer with two reflectors along the length of single mode fiber. The Fabry-Perot interferometer is a multiple beam interference device in which the output depends on the successive multiple reflections of an input beam between two mirrors which form a Fabry-Perot etalon. For a Fabry-Perot interferometer of cavity length L, the phase difference between the beams reflected from the first mirror and the second mirror is

$$\Delta\phi = \frac{4\pi nL}{\lambda} \tag{4}$$

One configuration utilizes cleaved fibers with an air gap between them to form a Fabry-Perot cavity [4]. In another configuration, the cavity is formed between a metal coated fiber and bare fiber [5]. Yet another configuration, known as the fiber Fabry-Perot interferometer (FFPI) sensor, the cavity is the section of fiber between two internal mirrors in the material of the fiber, as shown in Fig. 4.

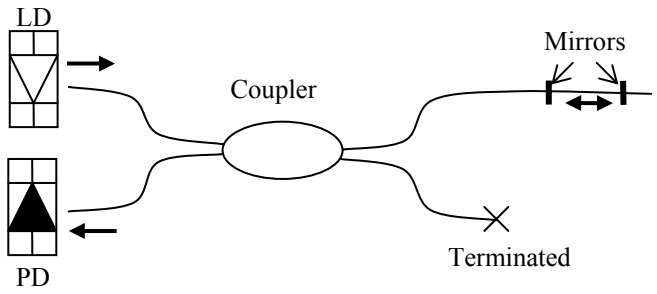

Fig. 4 Fiber Fabry-Perot interferometer.

Research on the FFPI sensor using a 1300 nm edge-emitting distributed-feedback (DFB) laser as the monitoring light source has been performed for over a decade in the Electrical Engineering Department at Texas A&M University [6]. Internal mirrors for these interferometers with reflectances in the 1%-10% range have been formed from a single layer dielectric film of TiO_2. Temperature sensing operation of FFPI sensors from -200°C to +1050°C has been demonstrated [7], and FFPI sensors have been embedded in graphite-epoxy composite and polymers where they were used to sense temperature [8] and ultrasonic pressure [9-10]. Multi-layers of TiO_2/ SiO_2 have been used to achieve

internal mirror reflectances as high as 86% [11]. Low coherent interferometery (LCI) using broadband light sources such as light emitting diodes (LEDs) has been researched [12,13]. FFPI sensor systems have been applied to measuring electrical current [14], in-cylinder pressure in engines [15-18], and strain in rails and in structures [19].

However, the high cost (~ $1000) of DFB lasers have limited the applications for which FFPI sensors are cost-effective. Less expensive lasers have been available for over a decade, but none of these inexpensive lasers emit in a single frequency (single mode) which is required for use with interferometric sensors such as the FFPI. The single mode vertical cavity surface emitting laser (VCSEL) is a low cost alternative to the DFB laser which emits in the 850nm spectral regime. Although VCSELs have been sold commercially for several years, making single mode VCSELs has proven difficult. Only recently have developmental samples become available from Honeywell.

I. B Research objective

This research represents, to the best of our knowledge, the first effort to apply VCSELs to the monitoring of interferometric fiber optic sensors. Spectral characteristics were measured for several VCSELs to determine combination of dc bias current, modulation current amplitude and modulation frequency for which single mode operation is achieved. Experiment in the monitoring of FFPI sensors were carried out using a variety of VCSEL operating conditions. The effect of optical feedback into the laser was also studied. Finally, the performances of 850 nm VCSEL/FFPI systems were compared with their 1300 nm DFB/FFPI counterparts.

CHAPTER II

FIBER FABRY-PEROT INTERFEROMETER (FFPI) SENSOR

II. A Theory

The fiber Febry-Perot interferometer (FFPI) is composed of two dielectric internal mirrors in a continuous length of optical fiber as shown in Fig. 5. The sensing region is localized between the two mirrors.

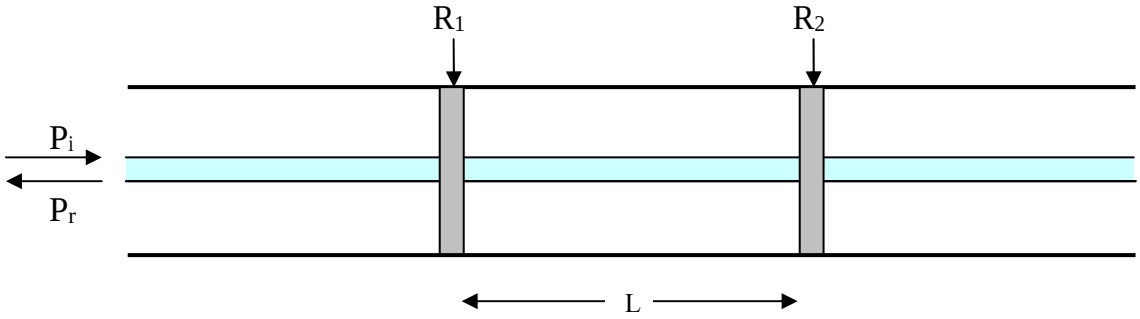

Fig. 5 Fiber Fabry-Perot interferometer structure.

The reflectance from the FFPI, R_{FP} can be written as

$$R_{FP} = R_1 + R_2 + 2\sqrt{R_1 R_2}\cos\phi = \frac{P_r}{P_i} \tag{5}$$

with mirror reflectances (R_1, R_2 << 1), P_r the reflected optical power, P_i the incident optical power, and ϕ the round-trip optical phase shift.

If the reflectance $R_1 = R_2 = R$, then R_{FP} in equation (1) can be expressed as

$$R_{FP} = 2R(1+\cos\phi) \tag{6}$$

The round-trip phase shift of the light inside the cavity of interferometer is given by

$$\phi = \frac{4\pi\nu nL}{c} = \frac{4\pi nL}{\lambda} \tag{7}$$

where ν is the optical frequency of the laser light, L is the cavity length of the interferometer, n is the refractive index of the fiber mode, c is the free-space speed of light, and λ is the free space wavelength of the light source.

The effect on ϕ of variations in length ΔL, frequency Δν and temperature ΔT can be expressed as

$$\phi = \phi_0 + \Delta\phi_L + \Delta\phi_\upsilon + \Delta\phi_T \tag{8}$$

with

$$\Delta\phi_L = \frac{4\pi\ n}{\lambda}\Delta L \tag{9}$$

$$\Delta\phi_\nu = \frac{4\pi L}{c}\left(n + \nu\frac{dn}{d\nu}\right)\Delta\nu \tag{10}$$

$$\Delta\phi_T = \frac{4\pi}{\lambda}\left(L\frac{d\nu}{dT} + n\frac{dL}{dT}\right)\Delta T \tag{11}$$

where ϕ_0 is the initial round trip phase shift.

If ϕ is $2N\pi \pm \frac{\pi}{2}$ (N = integer), the FFPI has a maximum sensitivity to the pressure. This is known as the quadrature condition. On the contrary, if ϕ is $2N\pi \pm \pi$ (N : integer), the sensitivity is zero. The sensor is typically monitored using a laser light source, as illustrated in Fig. 6.

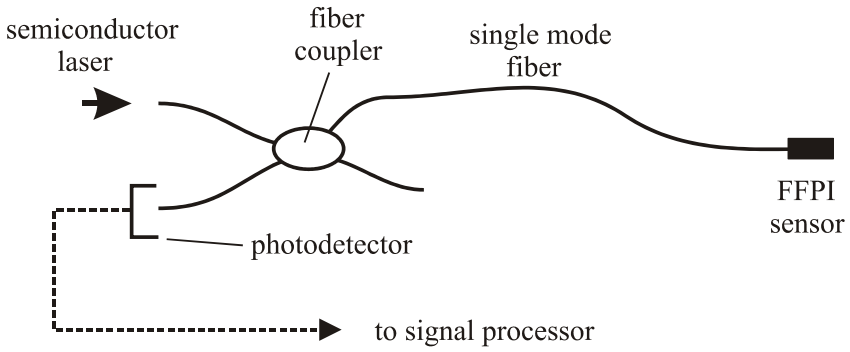

Fig. 6 Arrangement for monitoring an FFPI sensor.

Any physical perturbation which changes the optical length nL of the interferometer can be sensed. The reflected optical power as determined by interference of the reflected waves from two the mirrors, is converted to an electrical signal by a photodetector, and this signal is processed to obtain the value of the measurand of interest. Appropriately packaged FFPI elements can sense, for example, pressure, temperature, strain, liquid flow rate, and acceleration.

II. B Sensor fabrication

The sensors fabricated for this research were designed to operate in the 850 nm spectral regime to match the VCSEL emission spectral. By contrast, previous FFPI sensors have been designed for the 1300 nm range. Fiber for the 1300 nm sensors are multimode at 850nm, so FFPI sensors intended for operation at 1300 nm are not suitable for use with the 850 nm VCSELs. Fibers used in this research were single mode at 850 nm, meaning that they had a smaller core diameter than the 1300 nm single fibers.

The first step in the fabrication of an FFPI sensor is to strip the polymer buffer from a single mode fiber and cleave the end to produce a mirror surface perpendicular to the fiber axis. The fibers are placed in magnetron sputtering machine and coated with TiO_2 by vacuum deposition as shown in Fig 7. The reason for using TiO_2 is that it has high refractive index (~2.4, vs. 1.4 for the silica fiber) over visible and infrared spectral ranges and strong molecular bonding on glass based materials. The magnetron sputtering machine is filled with a mixture of 70% argon and 30% oxygen so that the titanium and oxygen atoms ejected toward cleaved fiber end and stick to the fiber until the desired film thickness is reached.

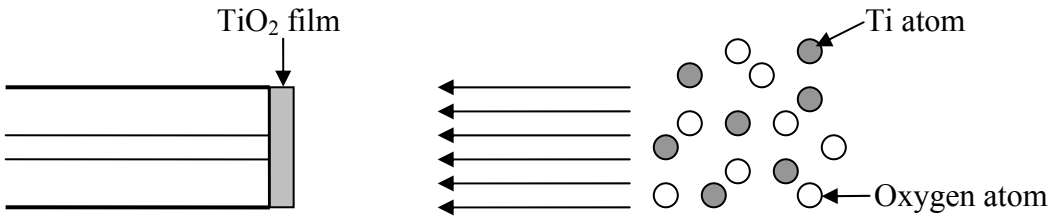

Fig. 7 Coating of bare fiber with TiO_2.

Since the TiO_2 will diffuse into the SiO_2 fiber during arc fusion splicing, the thickness of thin film should be chosen so that the TiO_2 mirror has maximum reflectance in the 850nm regime. As shown in Fig. 8, the TiO_2 film has a refractive index of 2.4 and the single mode fiber core has a refractive index of 1.458 at a wavelength of 850nm.

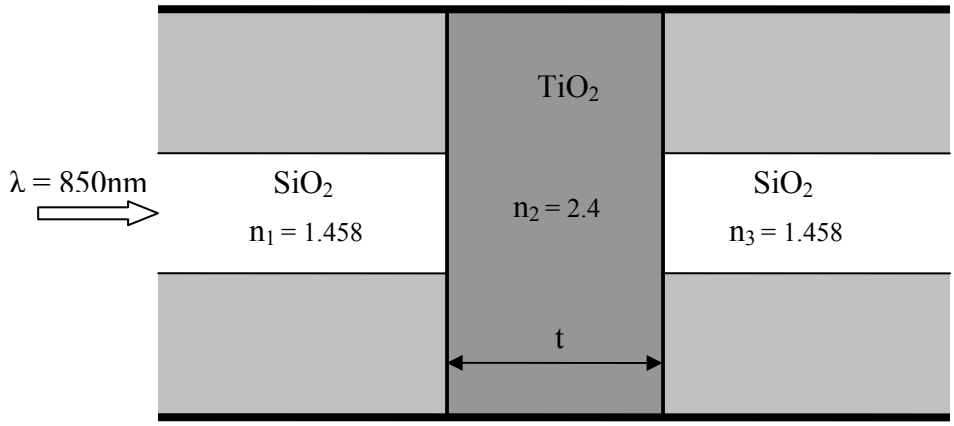

Fig. 8 TiO_2 film between single mode fiber.

The reflectance R of the internal mirror can be calculated using the equation

$$R = A_{12}^{\ 2} + A_{23}^{\ 2} + 2A_{12}A_{23}\cos\left(\frac{4\pi n_2 t}{\lambda}\right) \tag{12}$$

Where

$$A_{12} = \frac{n_1 - n_2}{n_1 + n_2} \tag{13}$$

and

$$A_{23} = \frac{n_2 - n_3}{n_2 + n_3} \tag{14}$$

Here, A_{12} and A_{23} represent the Fresnel reflection amplitudes for the two interfaces. Since in this case $n_3 = n_1$, it follows from these equation that $A_{12} = -A_{23}$. Fig. 9 and Fig. 10 show the relation between film thickness and reflectance at a wavelength at 850nm as calculated from equations (8)-(10).

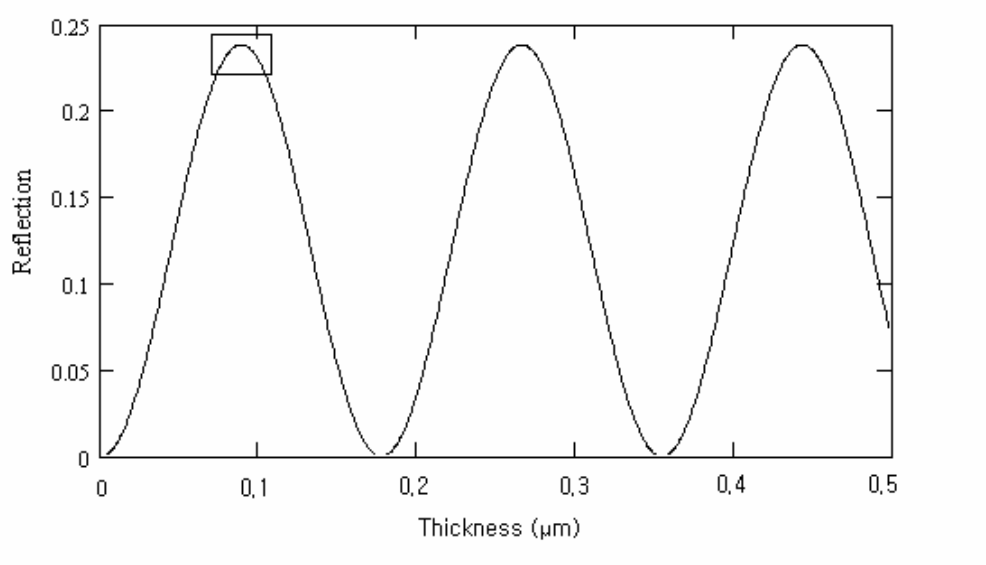

Fig. 9 Dependence of internal mirror reflectance on TiO_2 film thickness at a wavelength of 850nm.

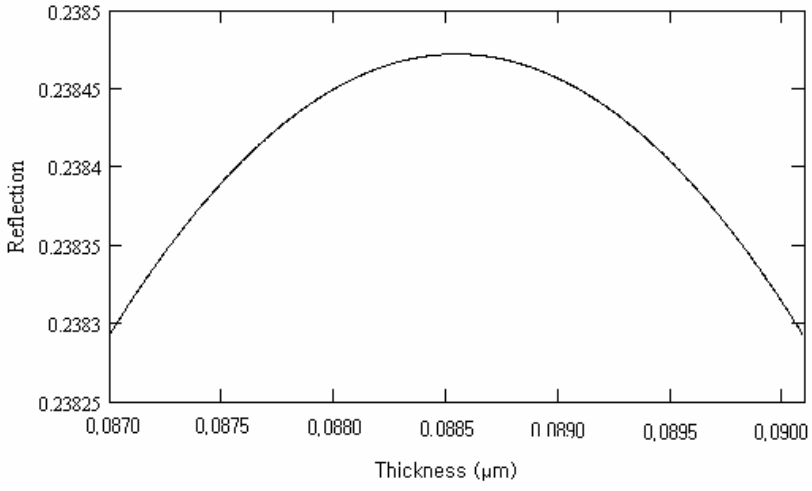

Fig. 10 First maximum in reflectance as a function of TiO_2 film thickness.

The maximum reflectance is predicted for a film thickness of 0.0885μm (88.5nm). During fusion splicing, the Ti atoms will diffuse into the fiber to some extent. By considering that the TiO_2 region will expand during splicing, a thickness of 85nm for the TiO_2 film coating is adequate for a wavelength of 850nm.

Using an arc fusion splicing technique, a coated fiber is spliced to a bare fiber. While monitoring the reflected power from the mirror, the arc is applied repeatedly until a mirror reflectance of ~5% is achieved. After producing one mirror, the fiber is cleaved at a distance of 12mm from first mirror and another thin film coated fiber is arc fusion spliced by the same method as the first splice so that the same reflectance can be achieved. The procedure is shown in Fig 11.

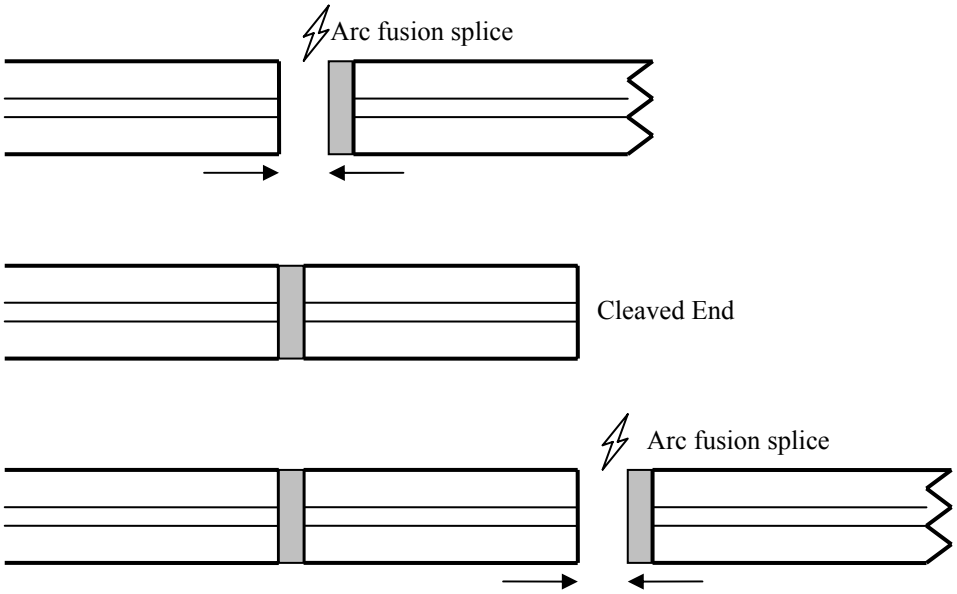

Fig.11 Arc fusion splicing of thin-film-coated fiber to produce an FFPI sensing element.

CHAPTER III

VERTICAL CAVITY SURFACE EMITTING LASER (VCSEL)

VCSELs are a relatively new kind of semiconductor laser. VCSELs were originally developed as a low cost alternative to Fabry-Perot (FP) and DFB Lasers. Unlike edge emitting semiconductor lasers, VCSELs emit light perpendicular to the broad planar surface of the wafer. The light is confined in the laser cavity, which is usually less than 2 wavelengths thick, using Bragg reflectors. These Bragg reflectors are multi-layer dielectric mirrors grown directly on the semiconductor surface as shown in Fig. 12. This mirror consists of alternate regions of high and low index of refraction layers. The distinguishing feature of this structure is the extremely short optical amplification region (on the order of 21nm). This length compares with the 300μm length typical of an FP or DFB laser. The mirror reflectivity is very high (~99%) so that a low-gain optical amplifier can achieve threshold. Only a single longitudinal mode is available for lasing because of the small distance between mirrors.

VCSELs were developed for telecommunication applications due to several advantages over edge-emitting laser diodes. They are cheaper to manufacture in quantity, easier to test, and more efficient in converting electrical power to optical power. They are inexpensive because they are completed and tested at the wafer level. In addition, the VCSEL requires less electrical current to produce a given coherent energy output, and low threshold currents enable high-density one- and two-dimensional surface-emitting arrays. The VCSEL emits a narrow, more nearly circular beam than traditional edge

emitters. Surface-normal emission and a beam pattern nearly identical to the geometry of the core of an optical fiber simplify alignment and packaging, and make it possible to couple light from the laser into an optical fiber with high efficiency.

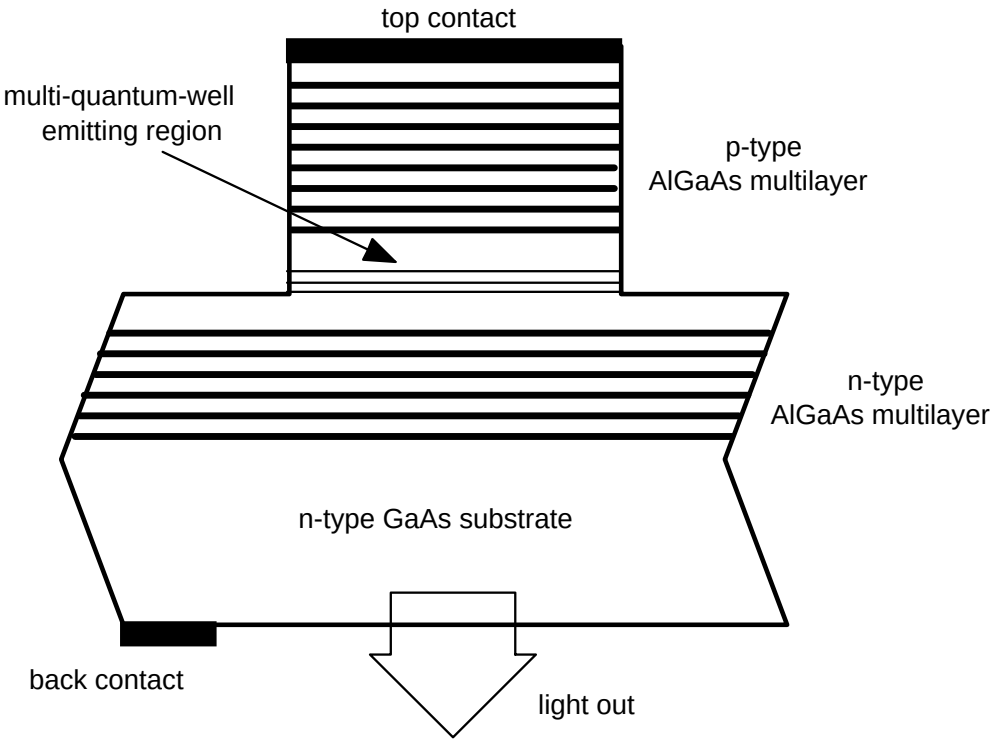

Fig. 12 Vertical cavity surface emitting laser (VCSEL). The AlGaAs multilayer comprise the Bragg reflectances which form the lasing cavity.

In this research, Advanced Optical Components (AdOpCo, formerly Honeywell) model SV3637 and SV3639-001 VCSELs are used. These emit in the 850nm wavelength regime with a threshold current of about 1 - 1.5mA, as indicated in the dependence of output power on current shown in Figs.13 and 15. Figs. 14 and 16 shows the spectra of these single mode VCSELs at a dc bias of 1.5mA.

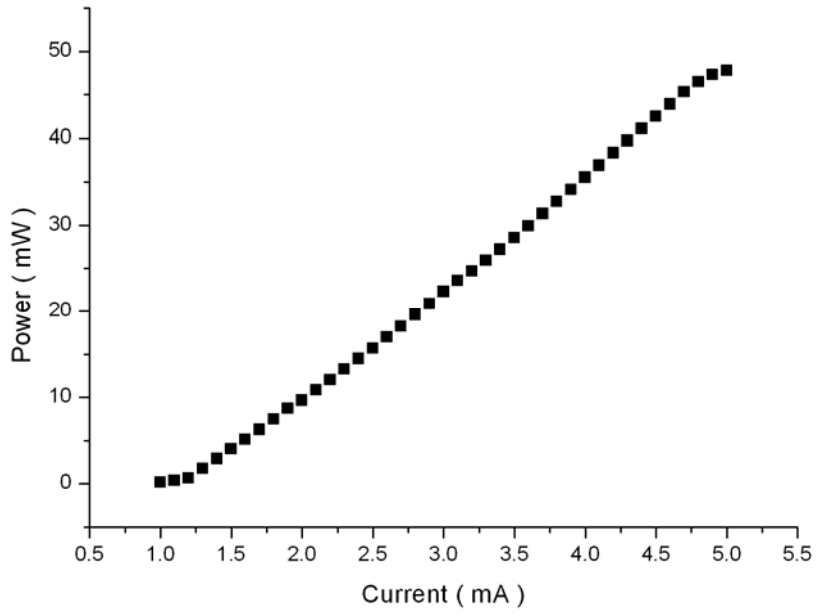

Fig. 13 Current VS power of AdOpCo SV3639-001 VCSEL.

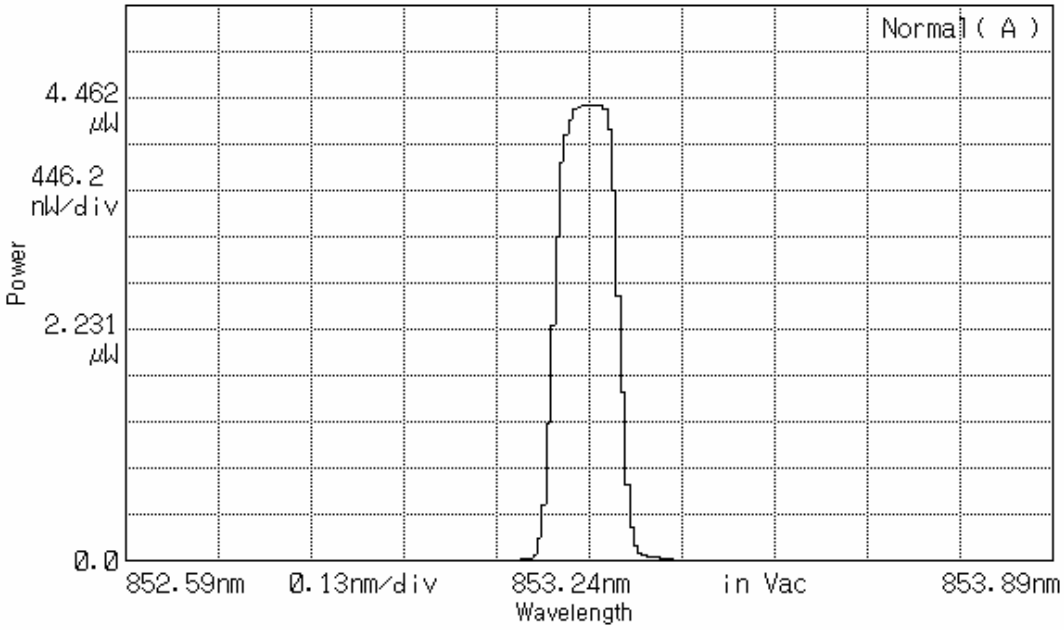

Fig. 14 Spectrum of single mode AdOpCo SV3639-001 VCSEL at 1.5mA dc bias current.

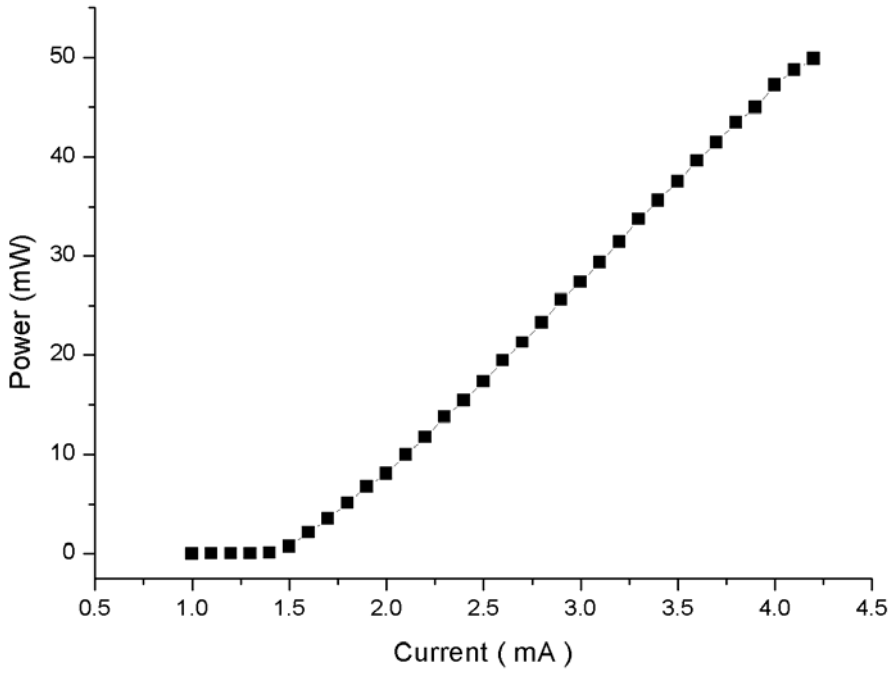

Fig. 15 Current VS power of AdOpCo SV3637 VCSEL.

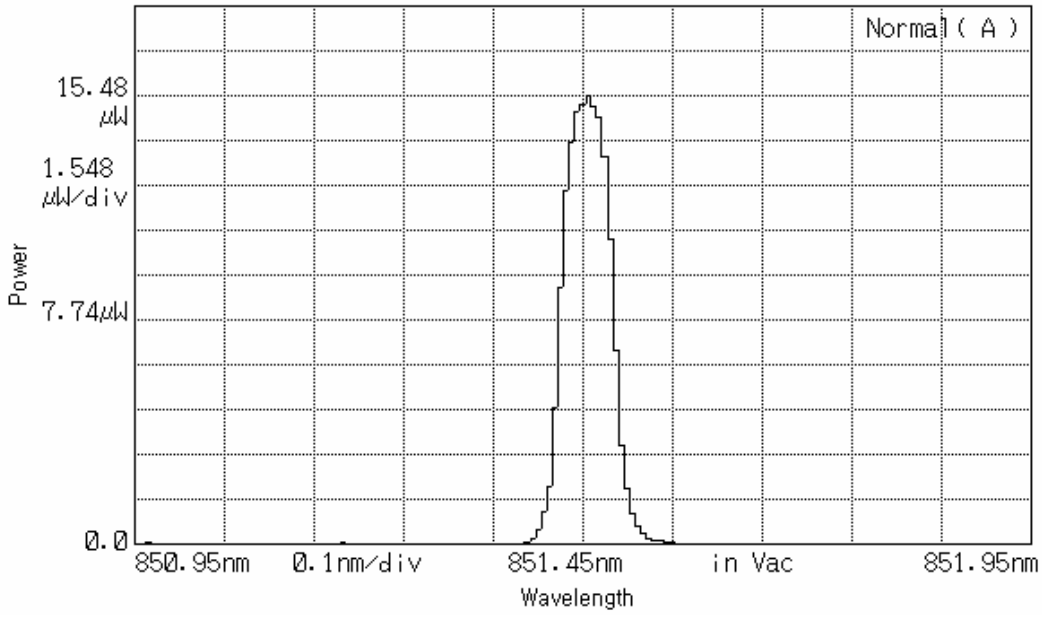

Fig. 16 Spectrum of single mode AdOpCo SV3637 VCSEL at 1.5mA dc bias current.

CHAPTER IV

EXPERIMENTAL INVESTIGATION OF VCSELs

Since the experiment uses an 850 nm VCSEL as light source, the thickness of TiO_2 deposition to achieve a desired mirror reflectance will be considerably different from previous sensors using a 1300 nm edge emitting laser. Since the fiber must be single mode at the operating wavelength, specialty 850 nm single-mode fibers are used instead of conventional SMF-28 fiber, which is single mode at 1300 nm but multimode at 850 nm. A 3dB coupler which is single mode at 850 nm must also be used. Table 1 shows properties of both fibers.

Table 1. Specification of 3M 820nm single mode fiber and Corning single mode fiber.

Properties	3M FS-SN-4224	Corning SMF-28
Operating wavelength	820 nm	1310 nm
Second mode cutoff wavelength	<780nm	<1260nm
Mode field diameter at operating wavelength	5.5 ± 0.5 μm	9.2± 0.5 μm
Maximum attenuation at operating wavelength	5.0 dB/km	0.5 dB/km
Nominal numerical aperture	0.12	0.13
Maximum core-clad offset	1 μm	0.5 μm
Cladding diameter	125 ± 2 μm	125 ± 1 μm
Outer primary buffer coating diameter	250 ± 15 μm	245 ± 5 μm
Operating temperature	-55 to 85 °C	-60 to 85 °C
Reflective index of core at operating wavelength	1.4580	1.4675

The VCSEL has low threshold current of about 1.0mA ~ 1.5mA. The manufacturer's rating for absolute maximum current is 5mA. It is very important that the current source not be allowed to exceed this maximum to avoid destroying the laser. A commercial current source for typical lasers is not appropriate for a low current. A simple 9V DC battery with a variable resistor in series to control the current is suitable, and it is also free from turn on voltage spikes which can occur in commercial power supplies. The VCSEL driving circuit to use in these experiments is shown in Fig. 17.

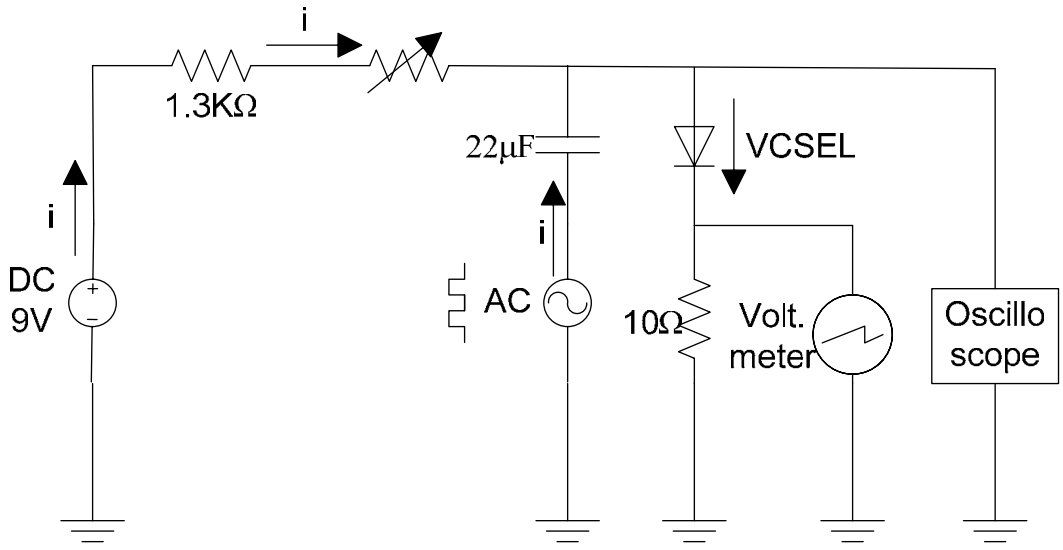

Fig. 17 VCSEL driving circuit.

The biasing and modulation of VCSEL should be carefully controlled. It should be biased just above the threshold current. It was found that when the VCSEL is modulated with a bias current above 2mA, it becomes multimode. Fig.18 shows the spectrum of a VCSEL driven with a 10kHz square wave with a modulation amplitude of

0.6mA and a 1.5mA DC bias current. Fig.19 shows a multimode spectrum of a VCSEL when driven at same modulation with 2mA DC bias current.

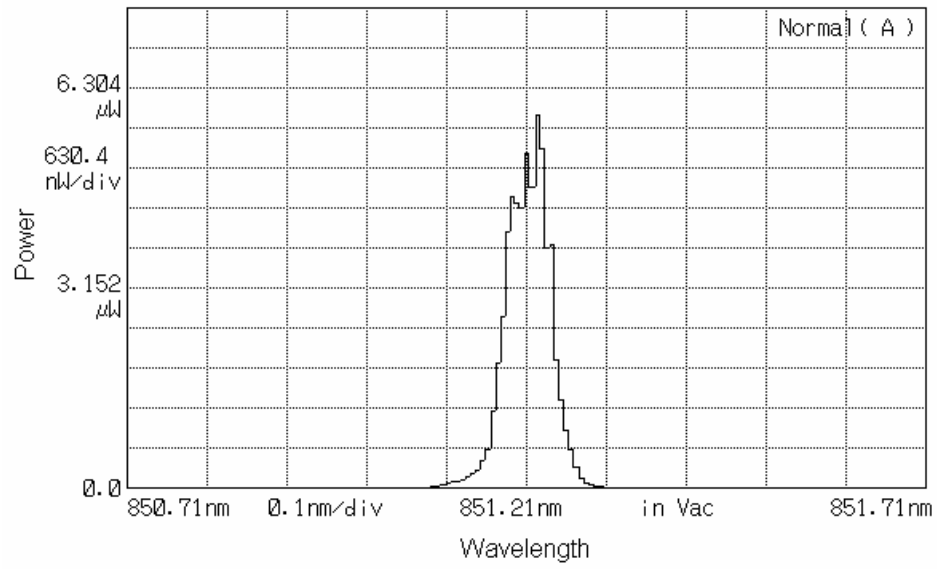

Fig. 18 Single mode operation spectrum of a VCSEL having bias current amplitude 1.5mA, modulation freq=10kHz, and modulation current = 0.6mA.

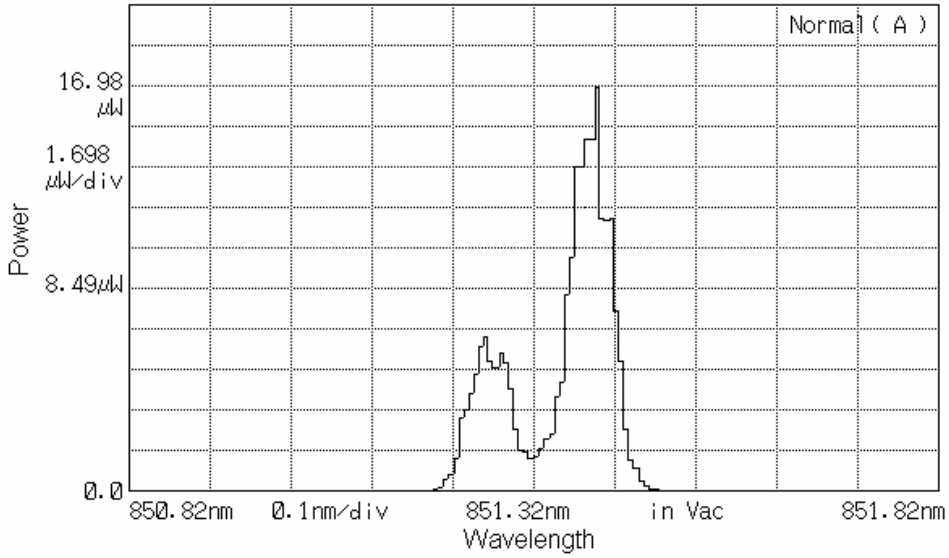

Fig. 19 Multi-mode operation spectrum of VCSEL having bias current amplitude 2mA, modulation freq=10Khz, and modulation current = 0.6mA.

CHAPTER V

EXPERIMENTAL INVESTIGATIONS OF FFPI SENSORS MONITORED WITH 850nm VCSELs

V. A Experimental investigation of FFPI sensors monitored with VCSELs

The experiment setup is shown in Fig. 20. Light from the VCSEL is coupled into the single mode fiber using two lenses. Since the light source has a wavelength of 850 nm, it is desirable to use lenses which are anti-reflection coated for this spectral regime. After entering the fiber the light passes through a 3dB fiber coupler to the FFPI sensor. A portion of the light reflected by the FFPI sensor impinges on the photodiode after passing again through the coupler. The reflected signal is displayed on an oscilloscope. To eliminate all reflections other than the one from the FFPI sensor, all fiber ends are angle polished or index matched. The sensor cavity length L is 12mm.

Monitoring of the FFPI sensor makes use of frequency modulation of the laser in response to a time-varying drive current. Reflected light from the FFPI varies with time to produce a “fringe” pattern in response to frequency modulation of the laser. In particular, it follows from eqs. (6) and (7) that a linear variation of laser frequency with time results in a sinusoidal variation of the FFPI reflectance with time. A change in the optical path length nL of the laser results in a shift in the fringe pattern.

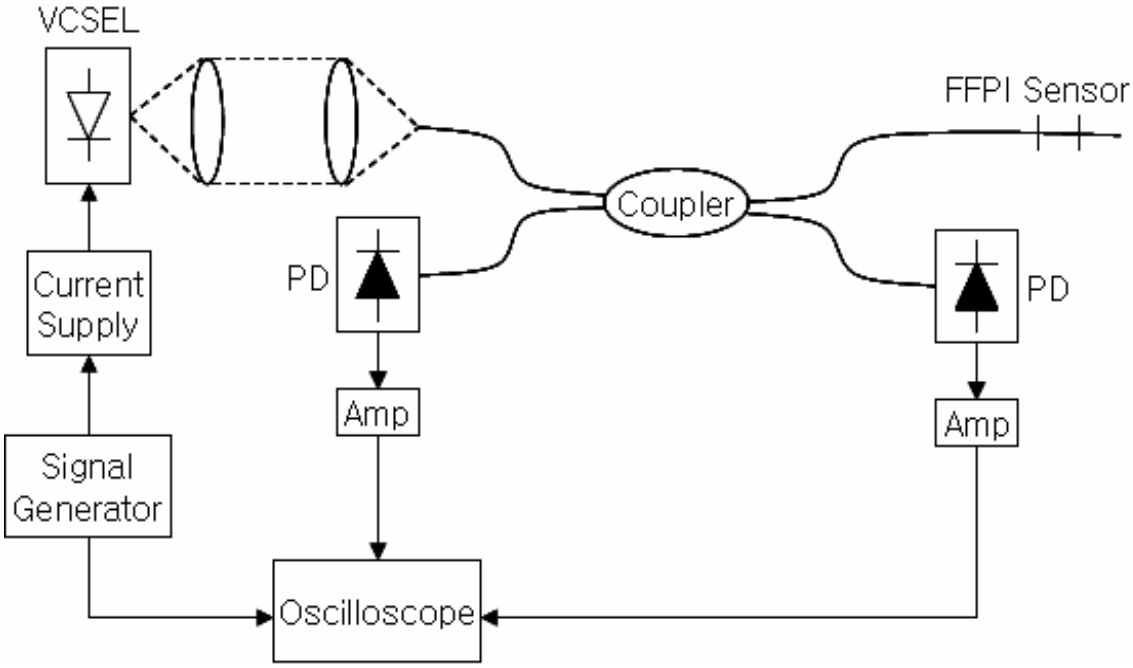

Fig. 20 Experiment setup for monitoring an FFPI sensor with a VCSEL as light source.

Response of an FFPI sensor monitored with a current–modulated, single mode VCSEL, model SV3639 manufactured by Advanced Optical Components, is shown in Fig. 21 for various bias currents. Square, triangular, and saw-tooth waveforms are applied at a frequency of 10 kHz with a modulation current of 0.6mA. As the bias current increases, the starting point of the fringes changes. To have a good fringe pattern, the bias current should be above threshold.

The effect of modulation current amplitude on the observed sensor response is shown in Fig.22. The fringe visibility is reduced considerably while the number of fringes is approximately doubled at the higher modulation current of 1.2mA. The

reduction in visibility results because the current below threshold for part of the cycle at the 1.2mA modulation amplitude.

The effect of increasing the modulation frequency is shown in Fig. 23. The frequency increase does not noticeably affect the fringe pattern except for the triangular wave at 10 kHz modulation. In that case, the lower part of the fringe envelope increases with bias current, due to the frequency limitation of the photo-detector amplifier.

A second VCSEL, designated SV3637, was also tested with the same setup. This VCSEL has a higher threshold current of 1.5mA than the previous VCSEL (1.2mA). Square, triangular, saw-tooth wave are applied with various combination of bias current, modulation current, and modulation frequency as shown in Fig 24, 25, and 26 respectively. The same fringe pattern is achieved as with the previous VCSEL.

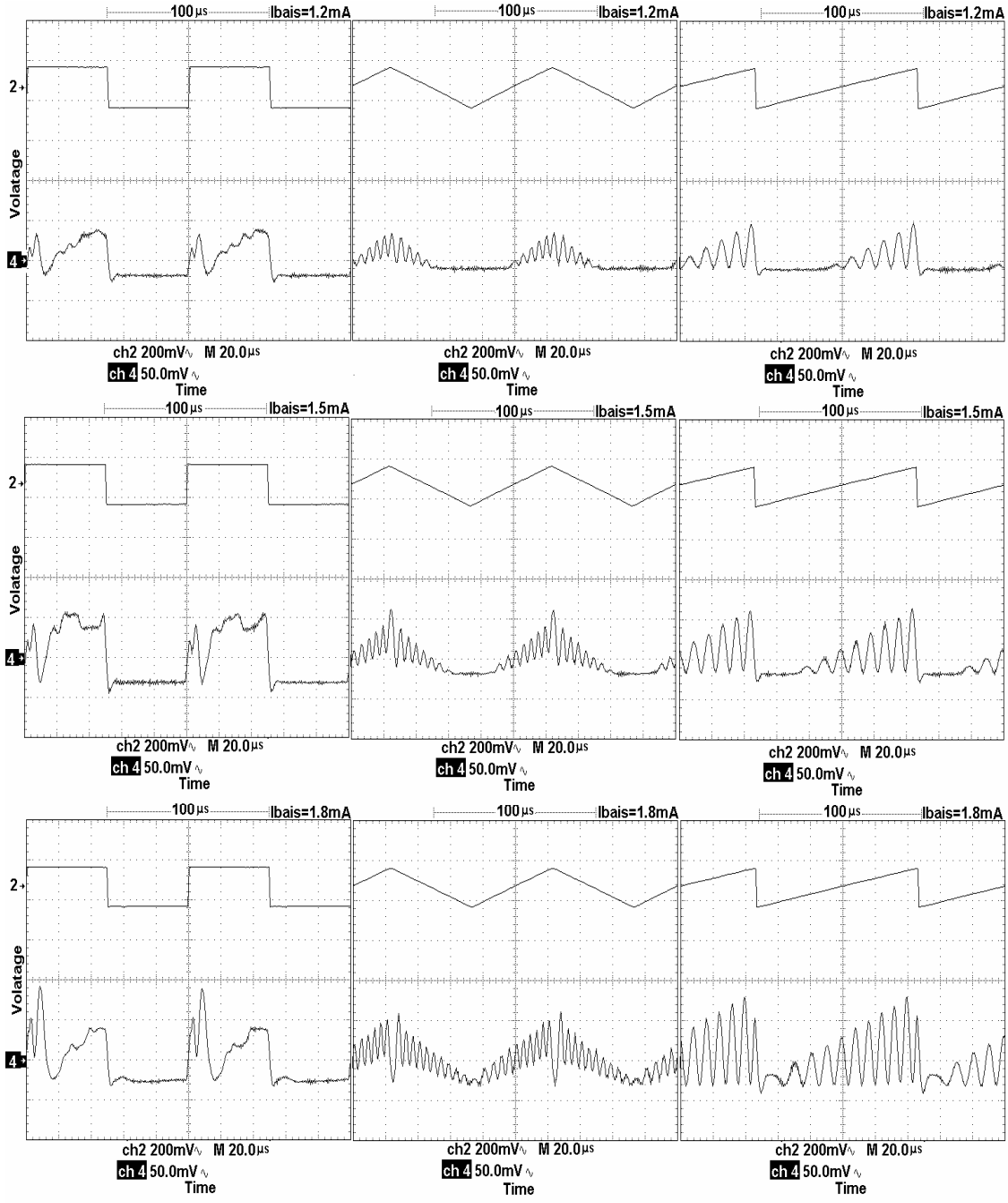

Fig.21 Temporal dependence of sensor output power using a SV3639 VCSEL light source for square, triangular, and saw-tooth modulating waveforms at different bias current levels. The first row traces are for bias current of 1.2mA, the second row traces are for 1.5mA, and last row traces are for 1.8mA. In each case the modulation peak to peak amplitude is 0.6mA, the horizontal scale is 20µs/div, and the modulation frequency his 10 kHz.

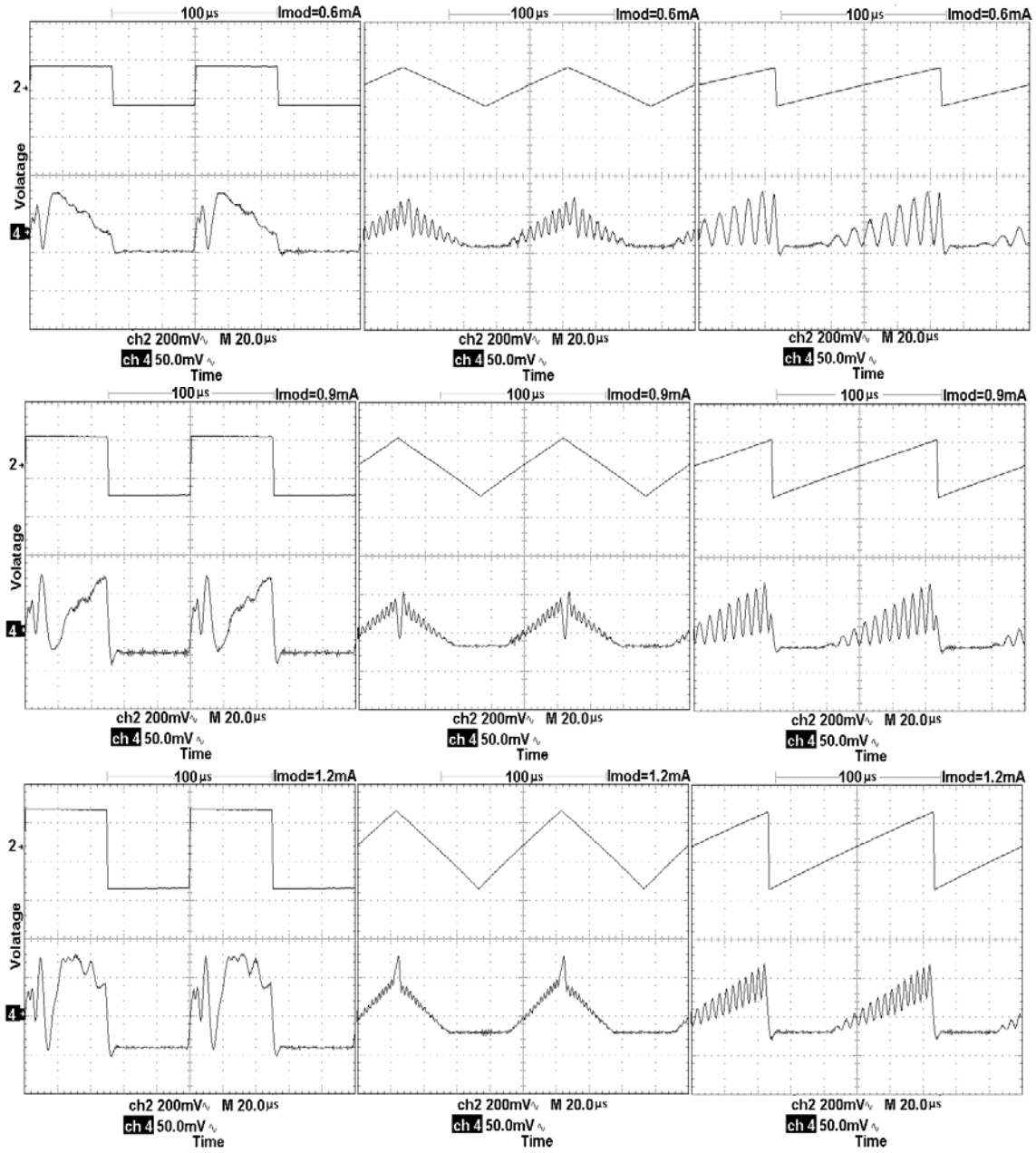

Fig. 22 Temporal dependence of sensor output power using a SV3639 VCSEL light source for square, triangular, and saw-tooth modulating waveforms at different modulation current levels. The first row traces are for modulation peak to peak amplitude of 0.6mA, the second row traces are for 0.9mA, and last row traces are for 1.2 mA. In each case the bias current is 1.5mA, the horizontal scale is 20µs/div, and the modulation frequency is 10 kHz.

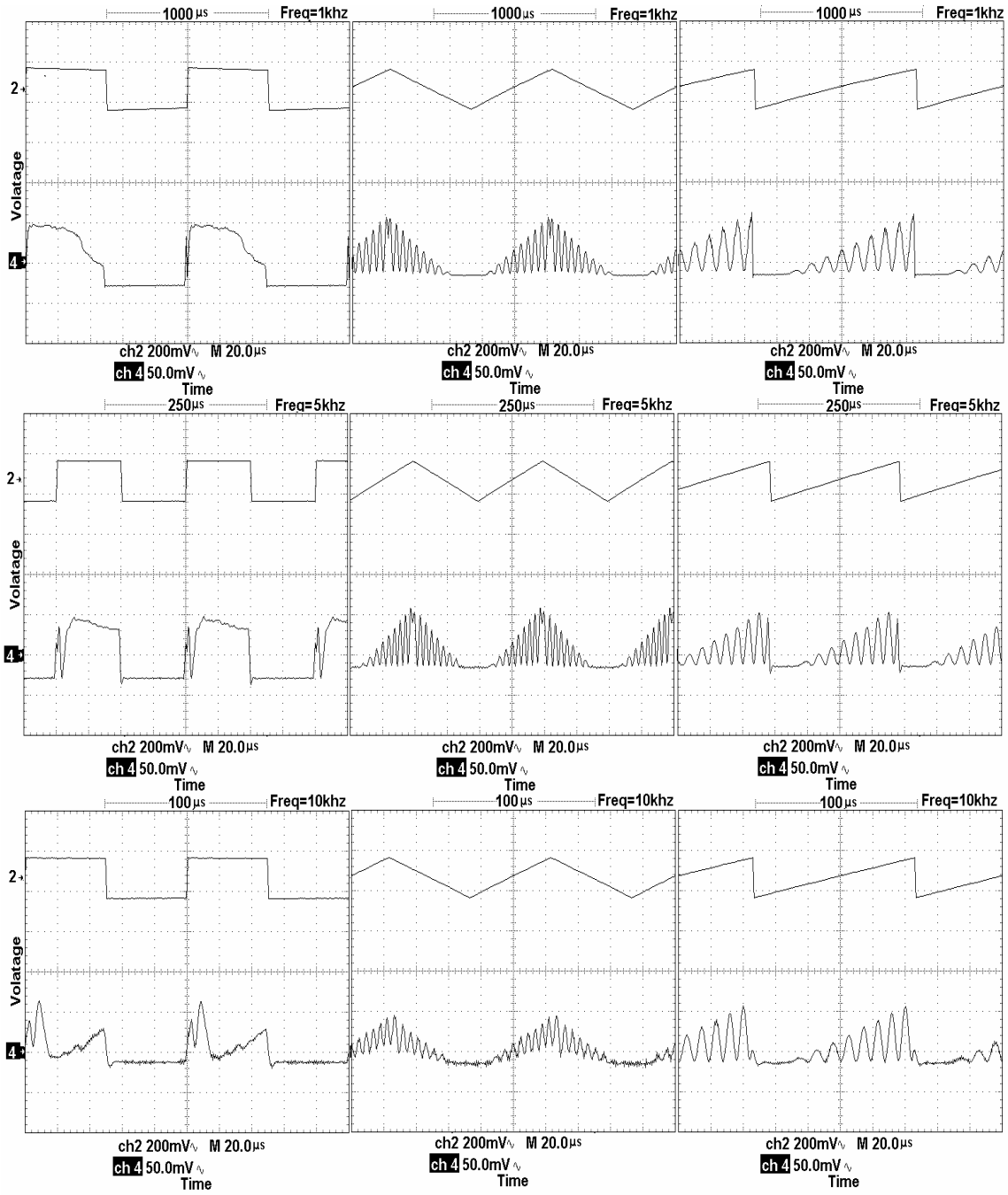

Fig. 23 Temporal dependence of sensor output power using a SV3639 VCSEL light source for square, triangular, and saw-tooth modulating waveforms at different modulation frequencies. The first row traces are for a modulation frequency of 1kHz, the second row traces are for 5kHz, and last row traces are for 10kHz with the horizontal scale of 200µs/div, 50µs/div, and 20µs/div respectively. In each case the bias current is 1.5mA, and the modulation peak to peak amplitude is 0.6mA.

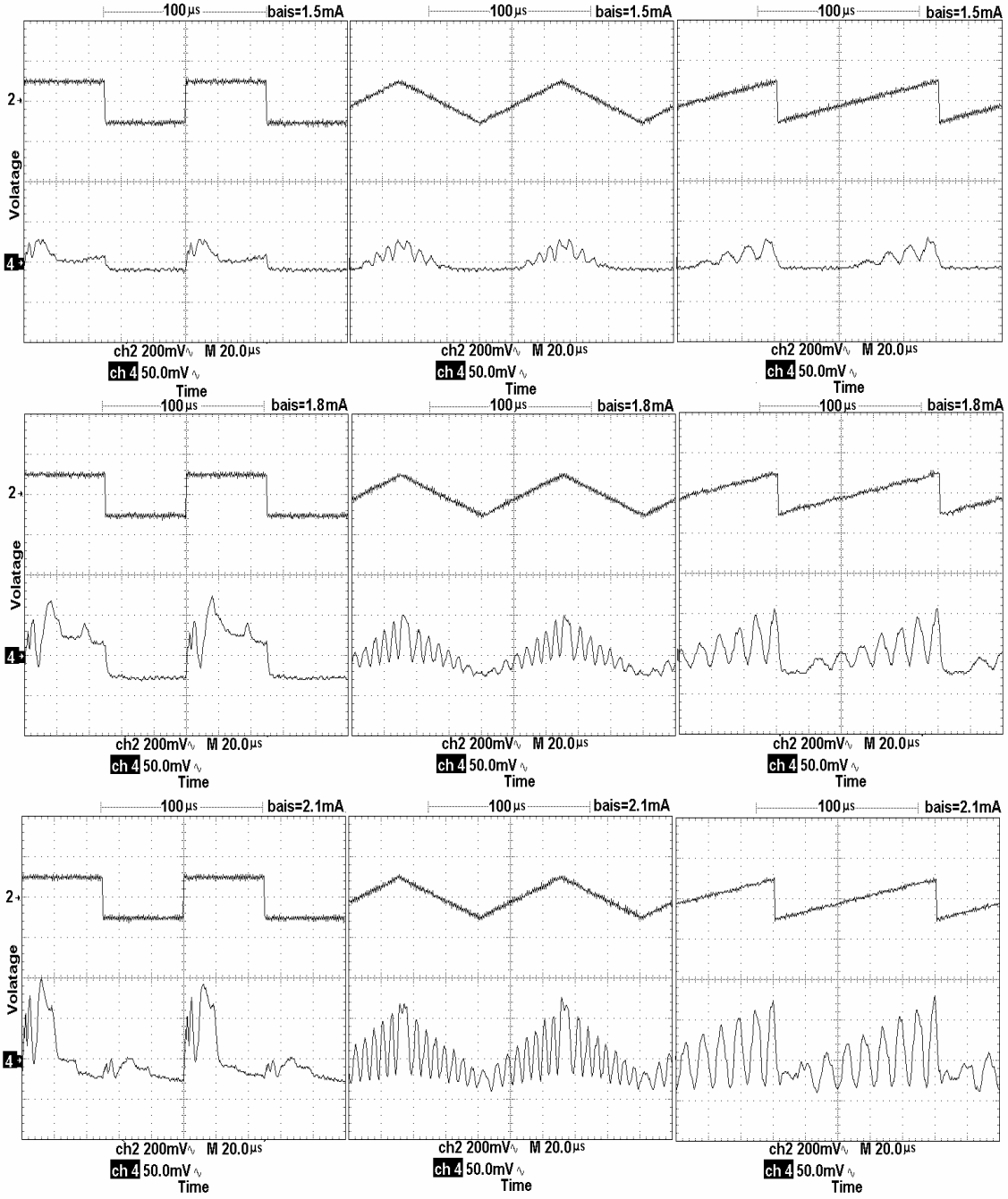

Fig.24 Temporal dependence of sensor output power using a SV3637 VCSEL light source for square, triangular, and saw-tooth modulating waveforms at different bias current levels. The first row traces are for bias current of 1.5mA, the second row traces are for 1.8mA, and last row traces are for 2.1mA. In each case the modulation peak to peak amplitude is 0.3mA, the horizontal scale is 20µs/div, and the modulation frequency is 10 kHz.

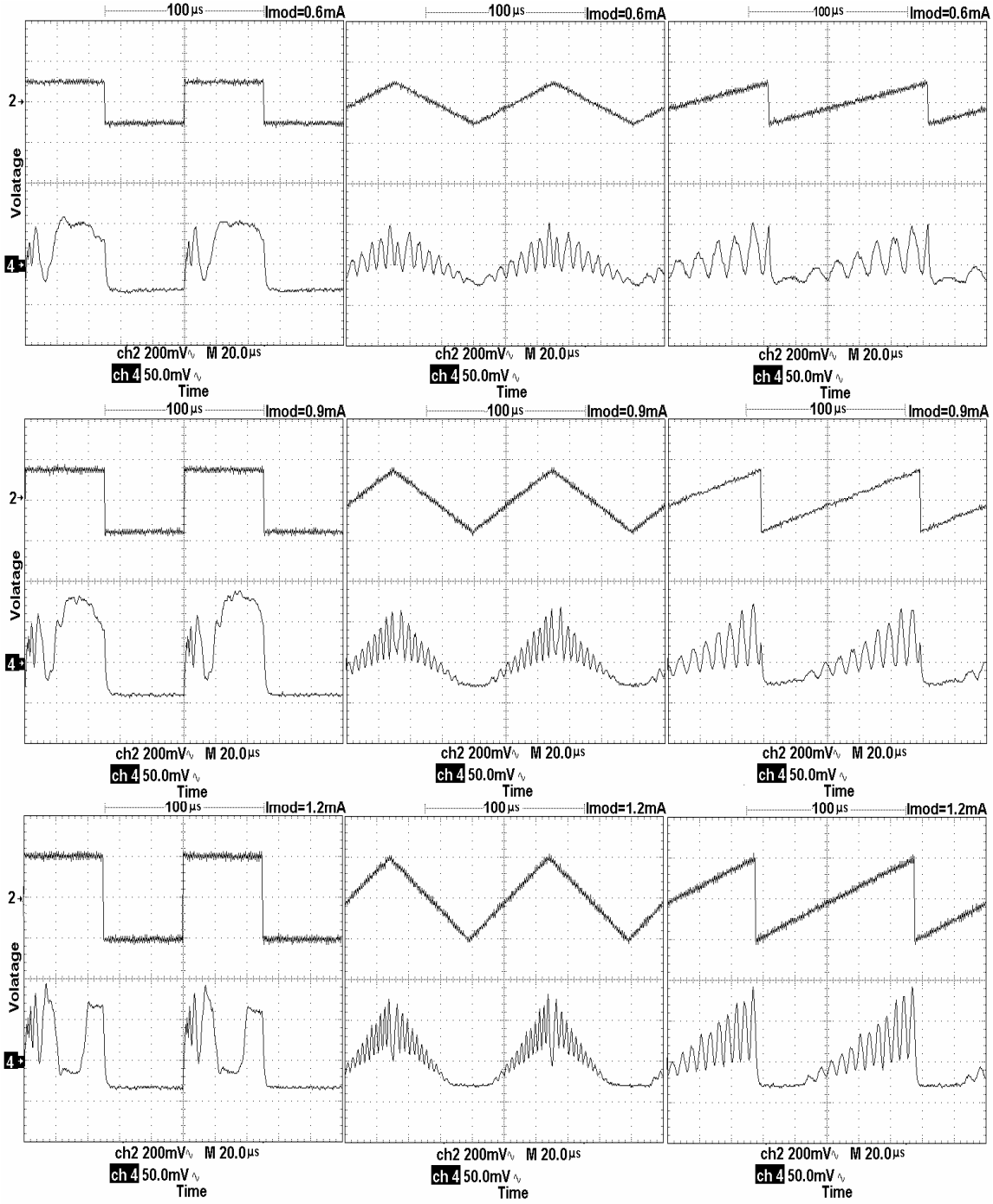

Fig. 25 Temporal dependence of sensor output power using a SV3637 VCSEL light source for square, triangular, and saw-tooth modulating waveforms at different modulation current levels. The first row traces are for modulation peak to peak amplitude of 0.6mA, the second row traces are for 0.9mA, and last row traces are for 1.2mA. In each case the bias current is 1.8mA, the horizontal scale is 20µs/div, and the modulation frequency is 10 kHz.

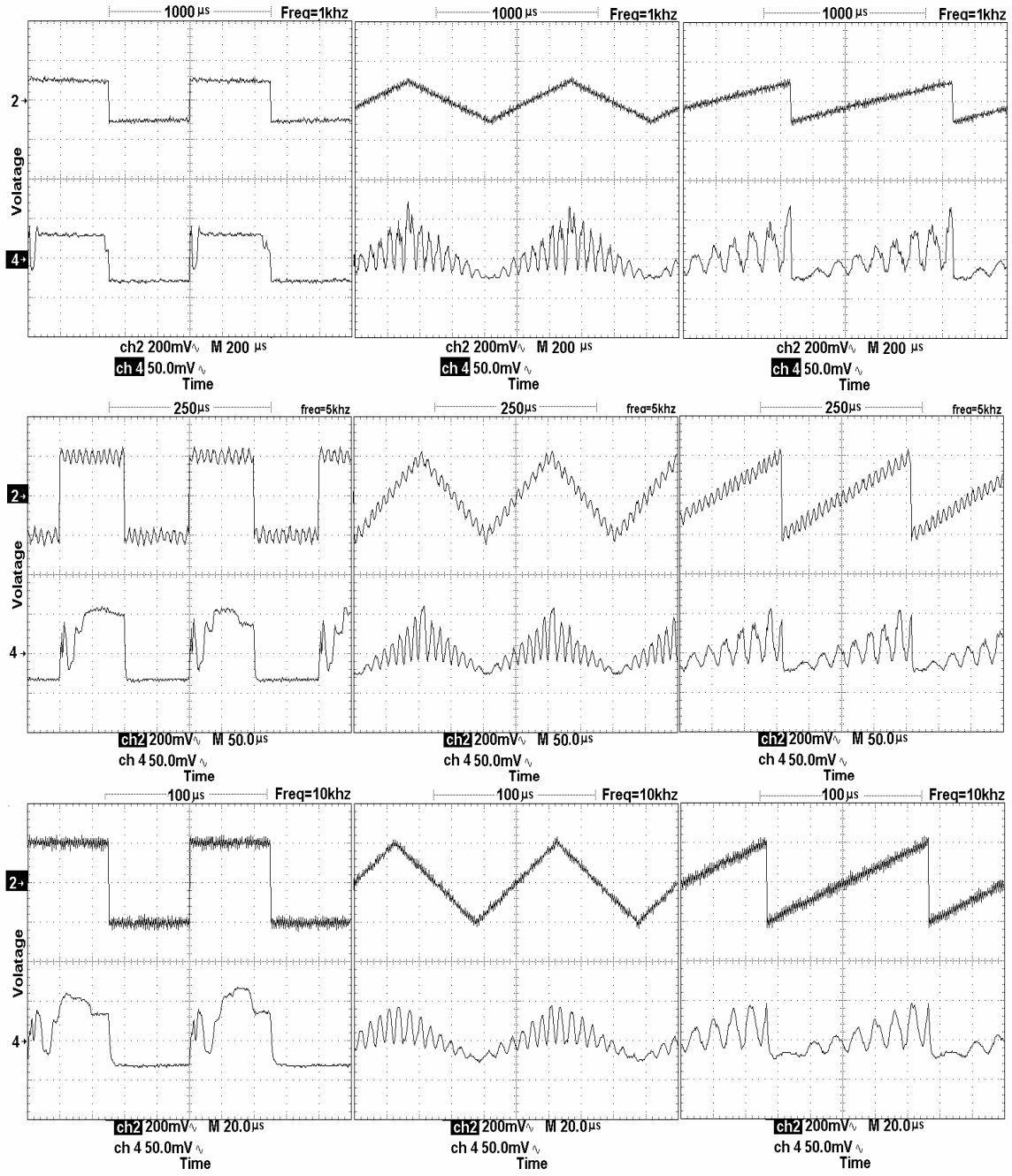

Fig. 26 Temporal dependence of sensor output power using a SV3637 VCSEL light source for square, triangular, and saw-tooth modulating waveforms at different modulation frequencies. The first row traces are for a modulation frequency of 1kHz, the second row traces are for 5kHz, and last row traces are for 10kHz with the horizontal scale of 200µs/div, 50µs/div, and 20µs/div respectively. In each case the bias current is 1.5mA, and the modulation peak to peak amplitude is 0.6mA.

V. B. Dependence of fringe patterns on VCSEL spectral characteristics

Due to the characteristics of the VCSEL, an FFPI sensor can operated properly only with certain combination of bias current, modulation current, and modulation frequency. Fig. 27 shows the region in which a VCSEL can operate with preferred fringe pattern when saw-tooth wave modulation with 10 kHz modulation frequency is applied. The circles represent the operable region, and the black dotted region represents multimode or improper fringe pattern.

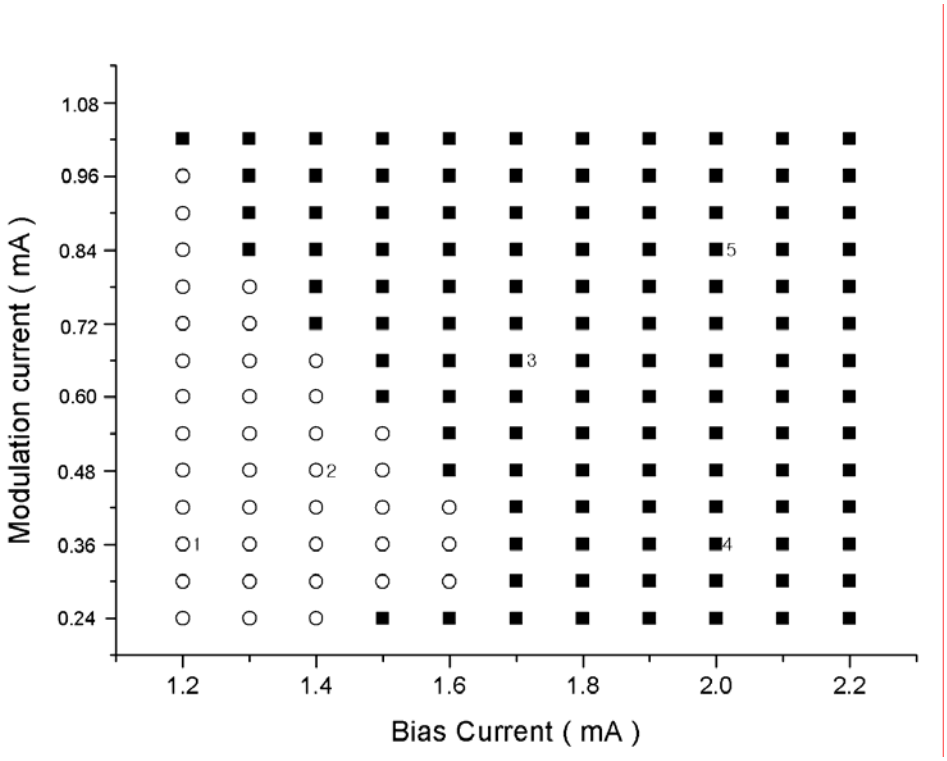

Fig. 27 Appropriate operating region for FFPI sensor with a SV3639 VCSEL.

The best operating point is designated #2 in Fig. 27. In region #1, the FFPI sensor is operable, but the bias current is so small that it yields only a small fringe

amplitude. In region #3, the fringe pattern looks workable, but the spectrum of the VCSEL tends to become multi-mode. In region #4, bias current is too high and the VCSEL becomes multi-mode. In region #5, both the bias current and modulation current are high, the fringe tends to lift up, and the VCSEL is multi mode. These numbered points indicated in Fig. 27 are shown in Figs. 28 and 29, with the fringe pattern and spectrum of VCSEL at each bias current and modulation current.

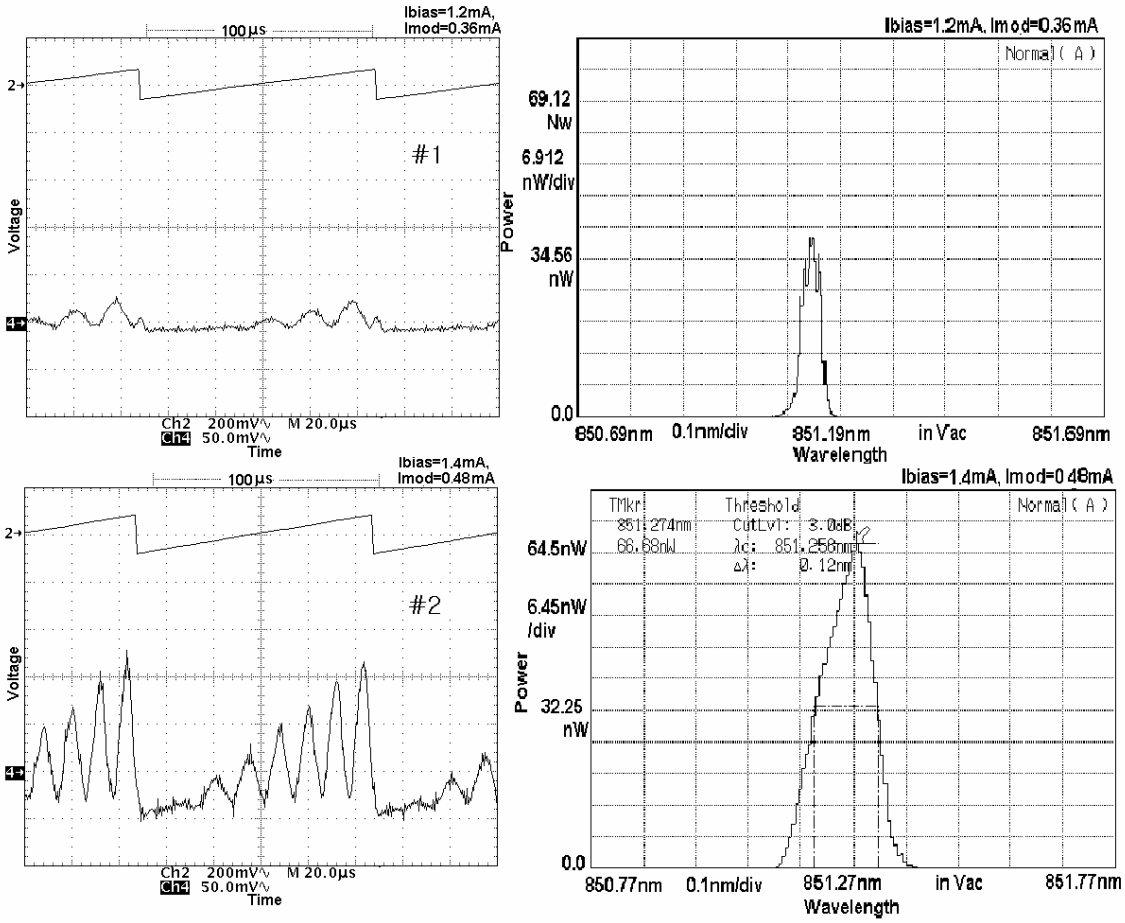

Fig. 28 FFPI sensor's fringe pattern and SV3639 VCSEL spectrum at each point indicated in Fig. 27.

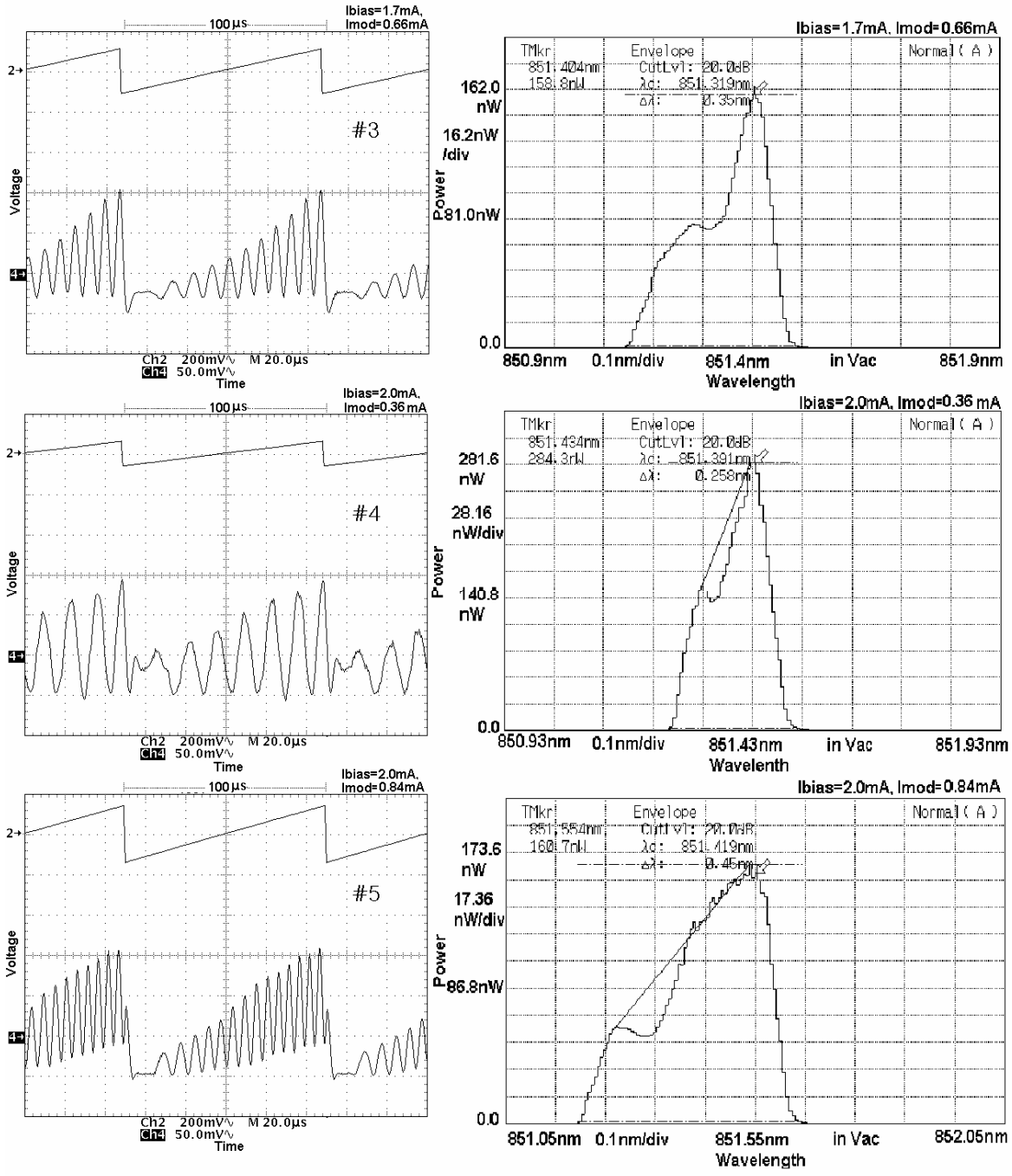

Fig. 29 FFPI sensor inoperable region's fringe pattern and spectrum of SV3639 VCSEL on each point indicated on Fig. 27.

V.C Operation of VCSEL/FFPI system at high modulation frequency and modulation depth

Since the VCSEL is designed originally for high speed data communication, FFPI sensors could be operated at high frequencies as well. Fig. 30 shows fringe patterns of the FFPI sensor and the VCSEL spectrum driven with a saw-tooth wave for frequencies of 10, 20, 50, and 100 kHz respectively. The high frequency fringe pattern is clearer than those at lower frequency. This may be because the VCSEL spectrum is narrower at high frequencies.

To observe the multi-mode behavior of a VCSEL with saw tooth wave modulation, the bias current was increased above the typical operating current of 1.5-1.8mA to cover a range from 2.0mA to 3.5mA in 0.5mA increment as shown in Fig. 31. As the bias current increases, the spectrum of the VCSEL becomes multimode and it is not suitable for FFPI sensor operation.

An increase in modulation current caused the number of fringes to increase. The spectrum of the VCSEL and fringe patterns with the modulation current increasing in increments of 0.2mA are shown in Fig. 32 with bias current and modulation frequency fixed at 1.8mA and 10kHz respectively. As the modulation current increases, the spectrum of the VCSEL broadens. This shows that these FFPI sensor will not operate well when the modulation current is too high.

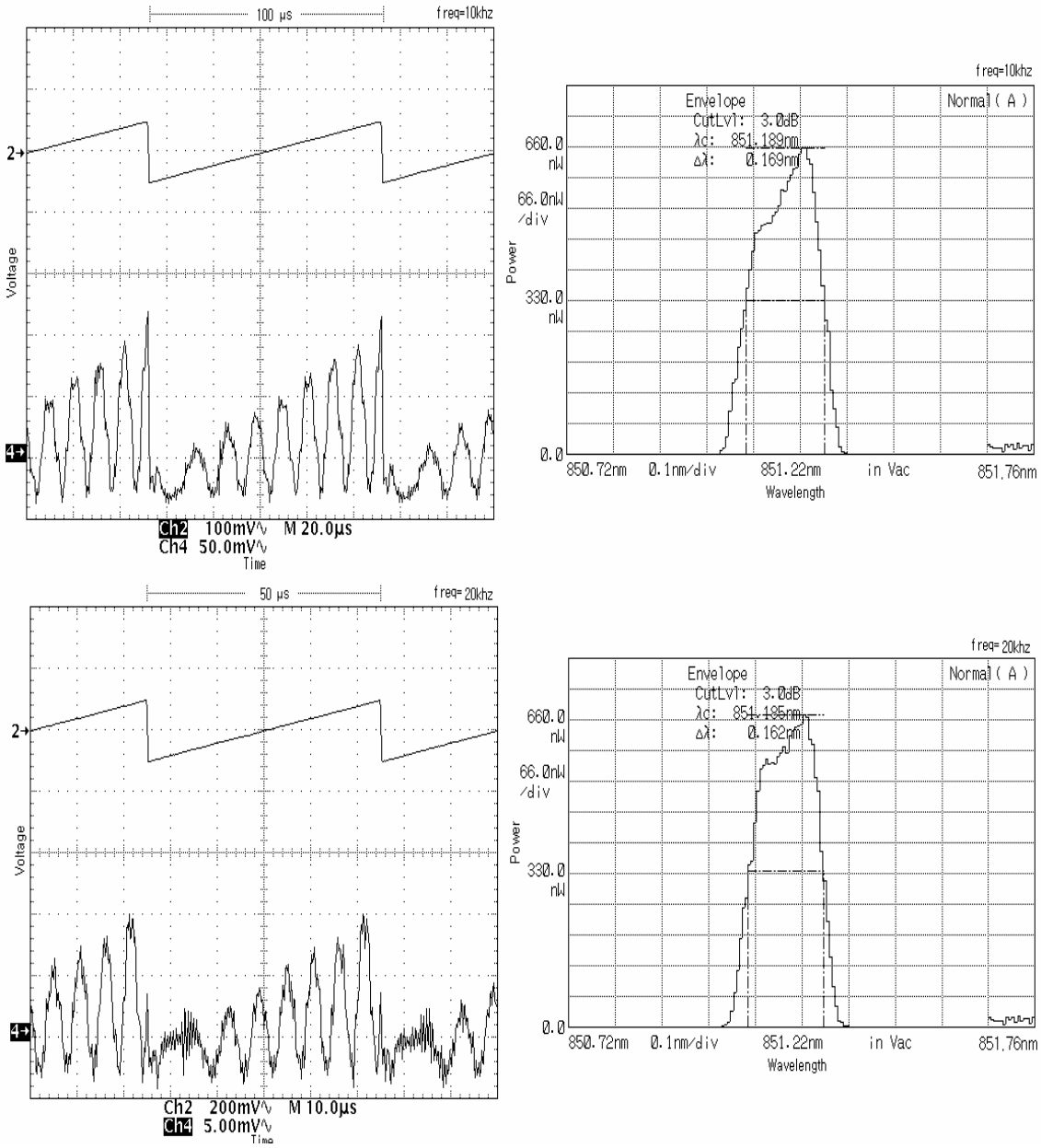

Fig. 30 Fringe pattern of FFPI sensor with SV3637 VCSEL modulation frequencies of 10, 20, 50, and 100kHz with a horizontal scale of 20µs/div, 100µs/div, 5µs/div, and 2µs/div from top to bottom respectively. Bias current is 1.8mA and modulation current is 0.6mA.

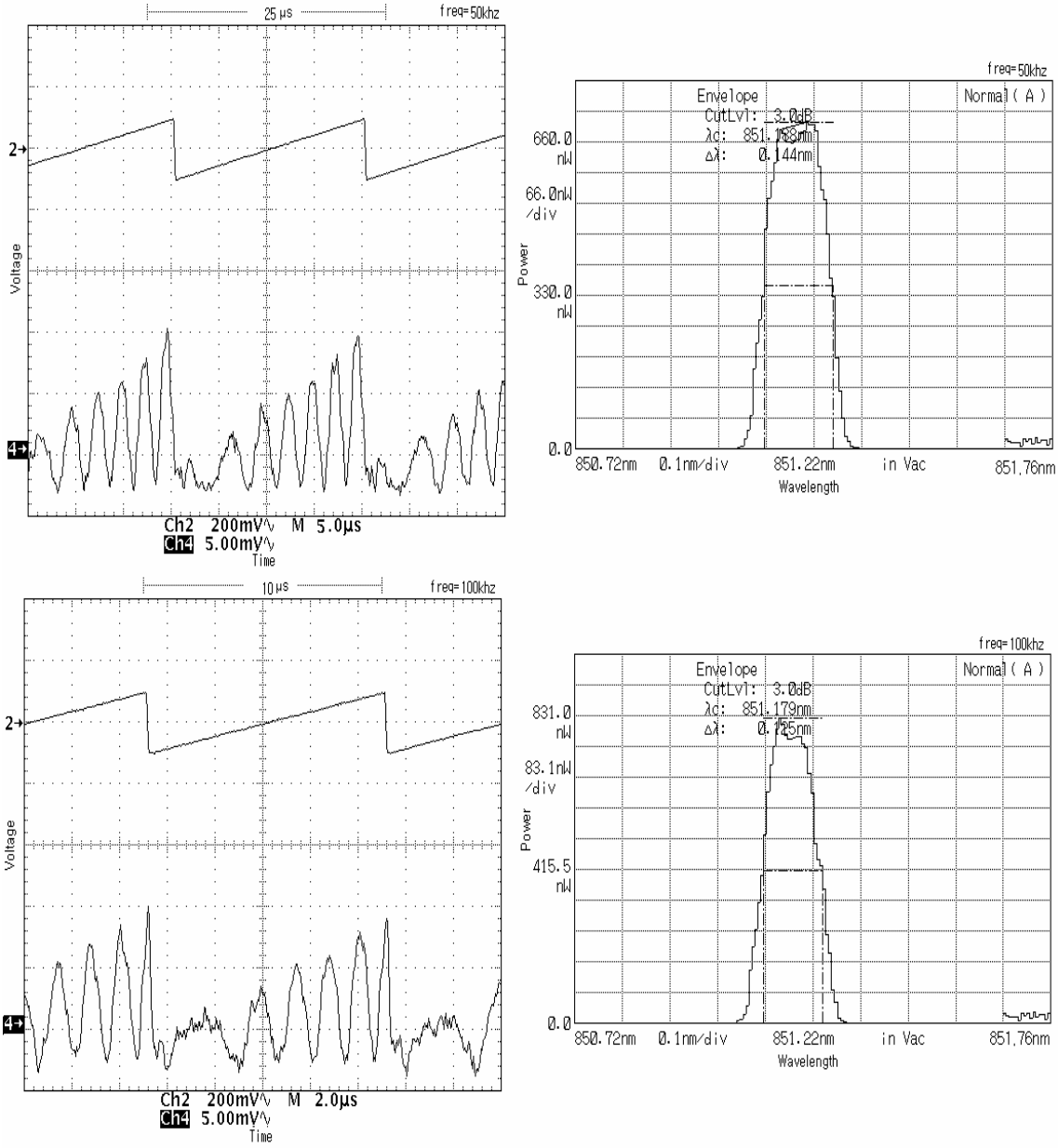

Fig. 30 (continued)

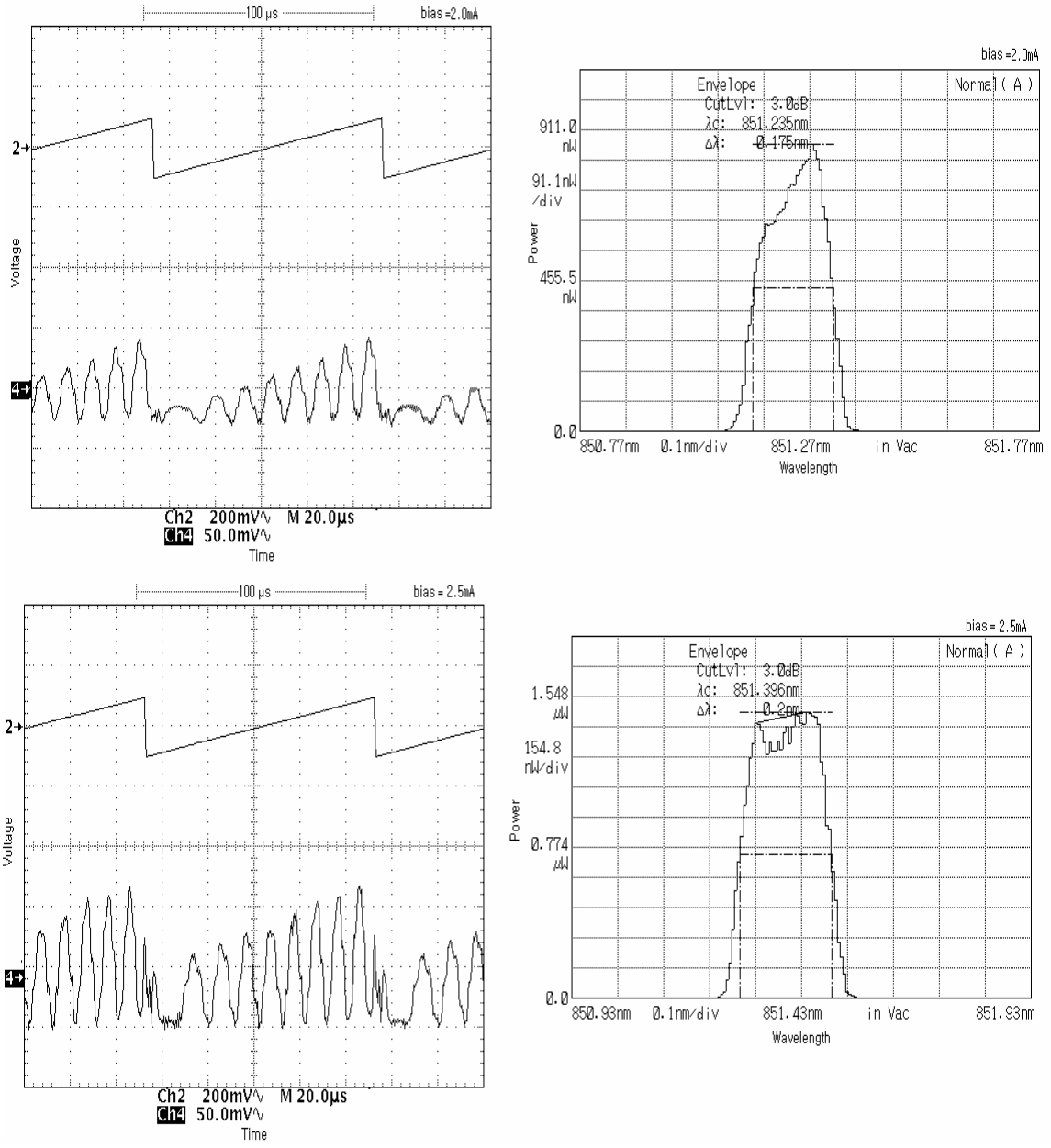

Fig. 31 Fringe pattern of FFPI sensor with SV3637 VCSEL on bias currents of 2, 2.5, 3, and 3.5mA from top to bottom respectively. Modulation frequency is 10 kHz, the horizontal scale is 20µs/div, and modulation current is 0.6mA.

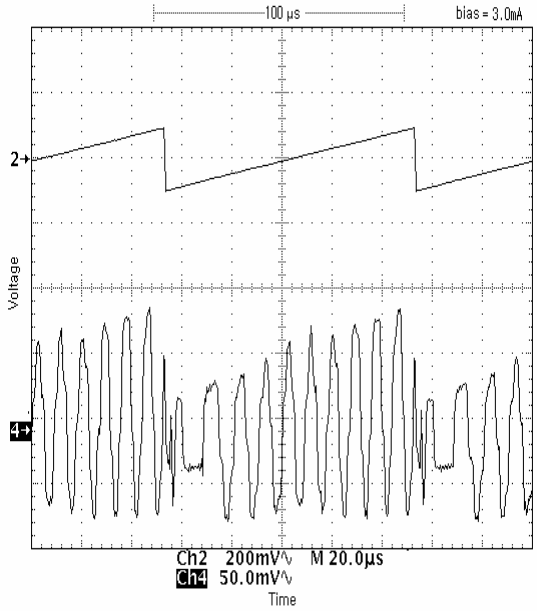

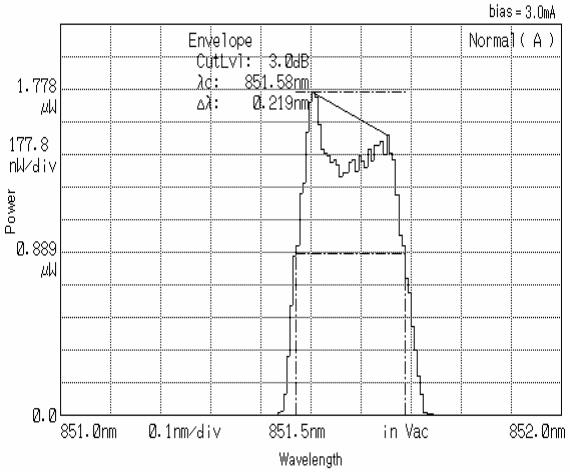

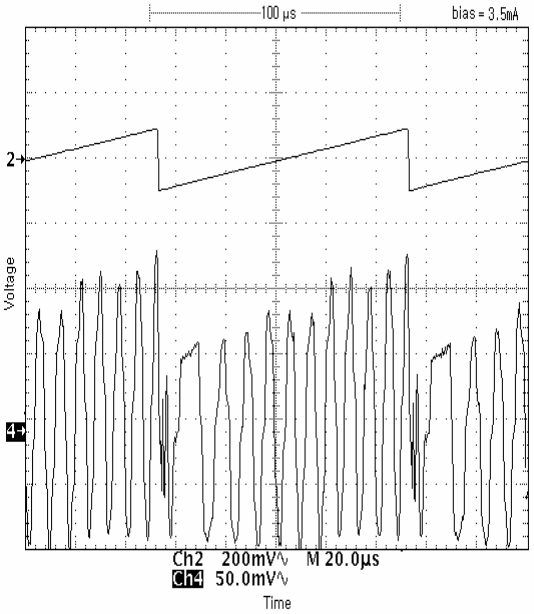

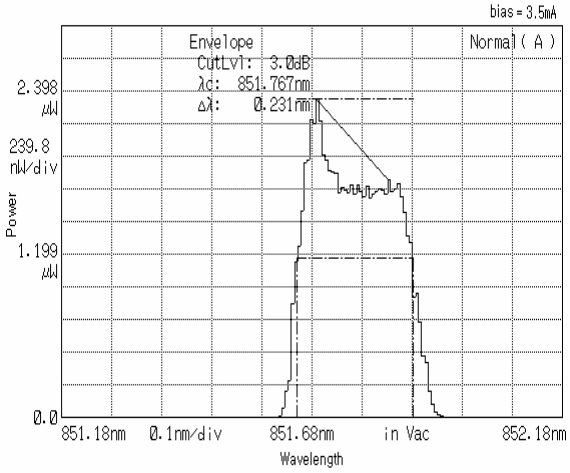

Fig. 31 (continued)

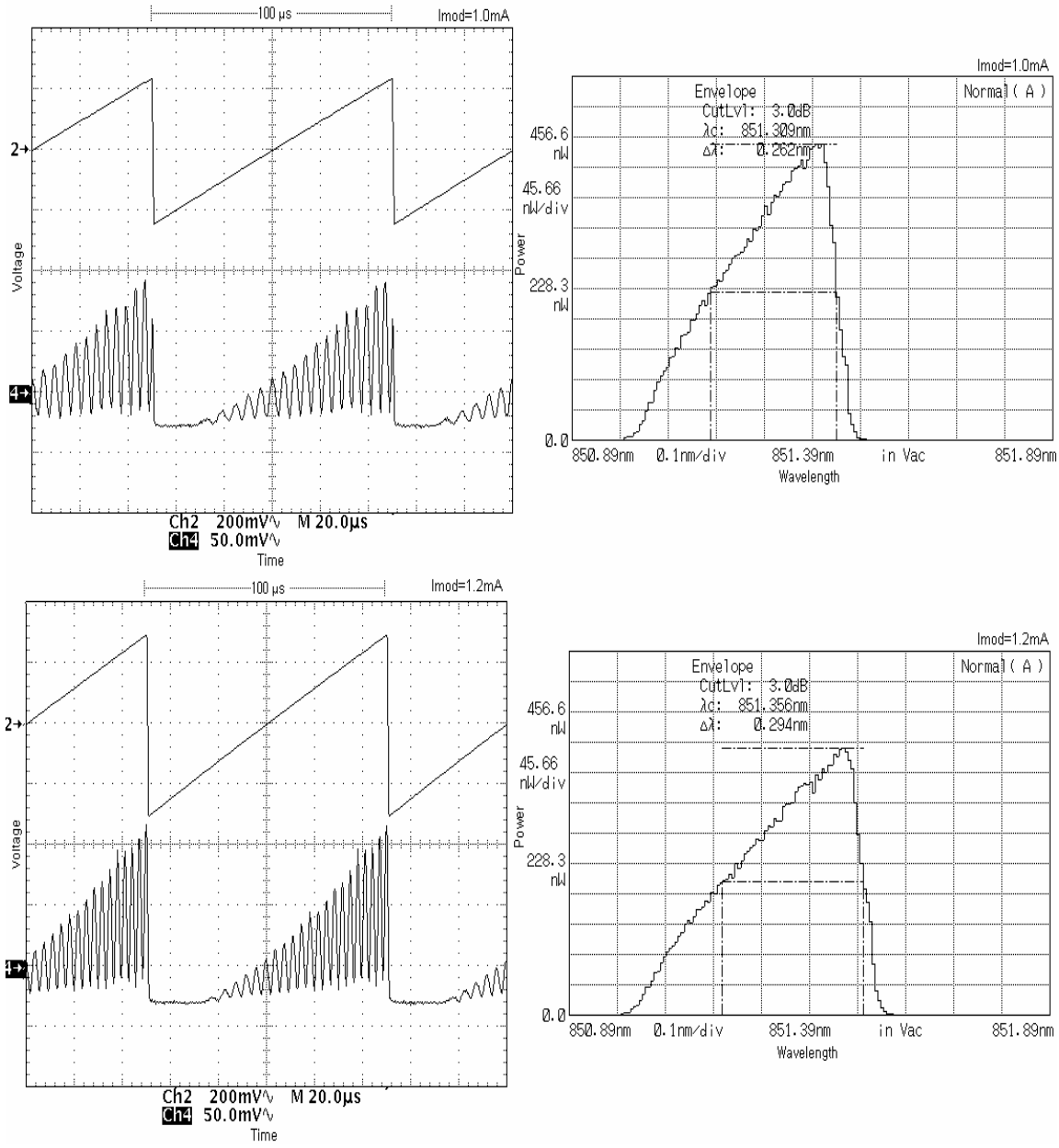

Fig. 32 Fringe pattern of FFPI sensor with SV3637 VCSEL at modulation currents of 1.0, 1.2, 1.4, and 1.6mA from top to bottom respectively. Modulation frequency is 10 kHz, the horizontal scale is 20µs/div, and bias current is 1.8mA.

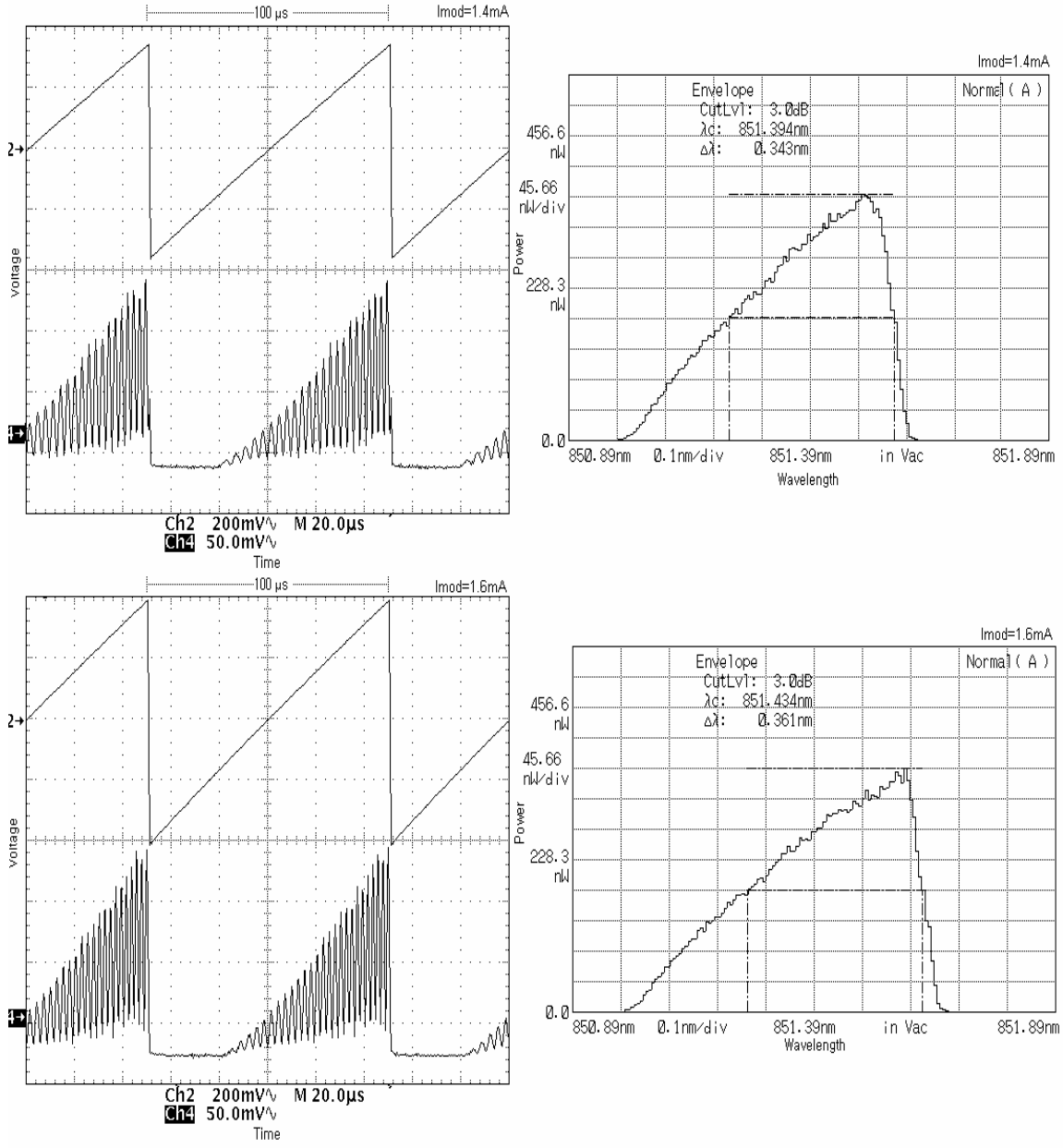

Fig. 32 (continued)

To investigate higher frequency operation of FFPI sensors with VCSELs, not only has the modulation current has been increased gradually but also the modulation frequency was increased to 20 KHz and 50 KHz as shown in Figs. 33 and 34. The loss of extinction in the fringe pattern is due to the frequency limit of the optical receiver.

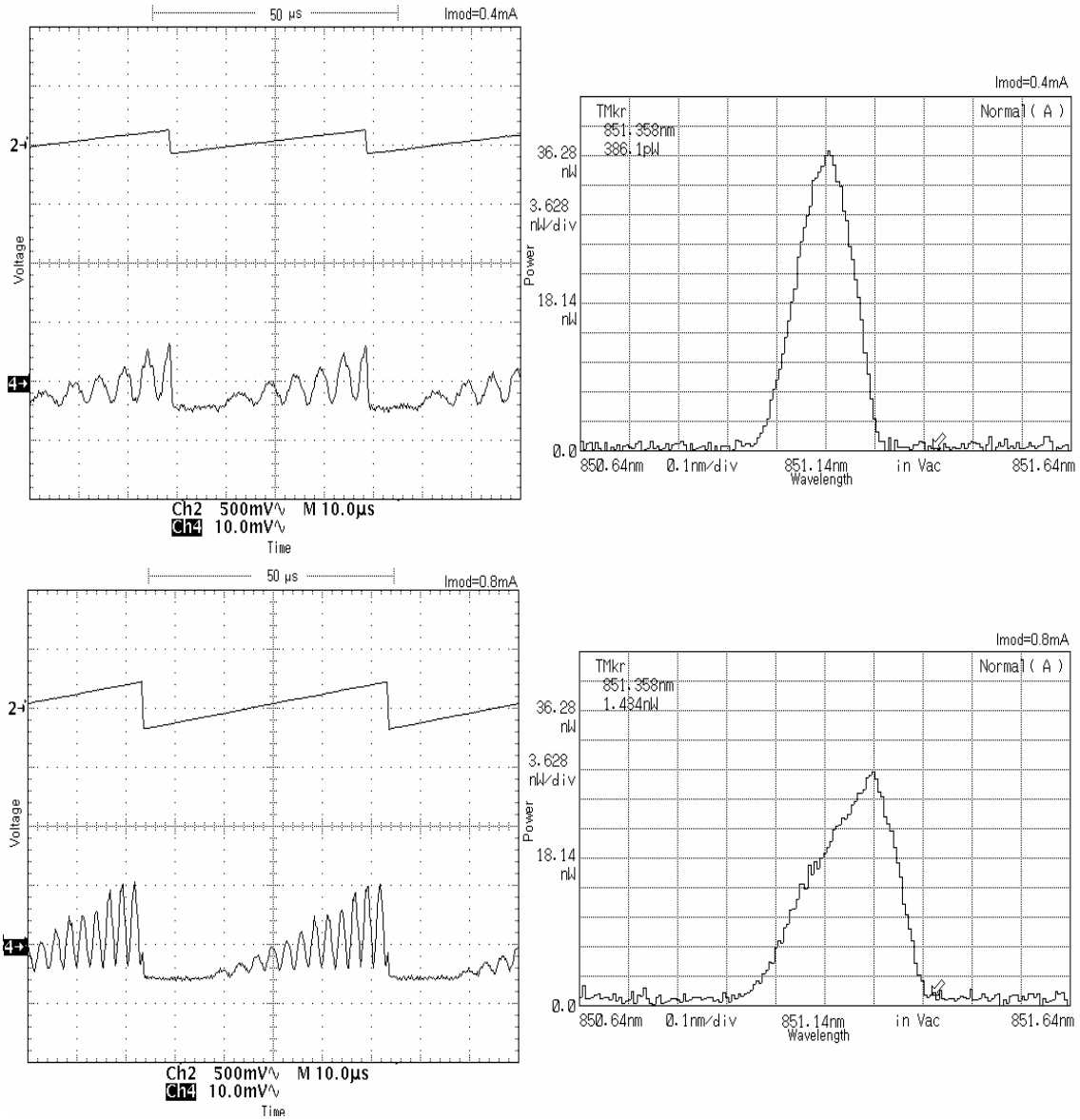

Fig. 33 Fringe pattern of FFPI sensor with SV3637 VCSEL at modulation currents of 0.4, 0.8, 1.2 and 1.6mA from top to bottom respectively. The modulation frequency is 20 kHz, the horizontal scale is 10µs/div, and the bias current is 1.8mA.

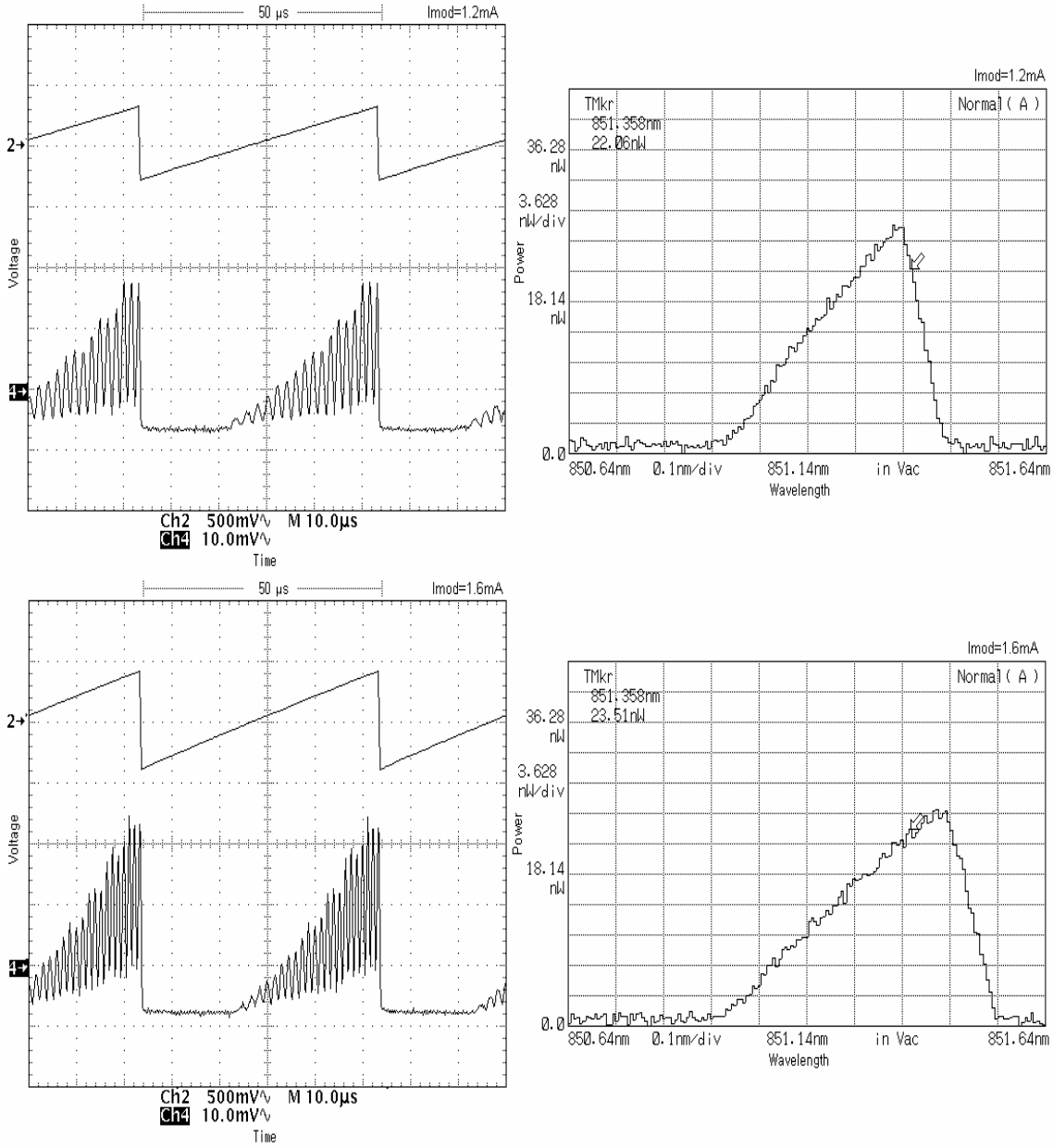

Fig. 33 (continued)

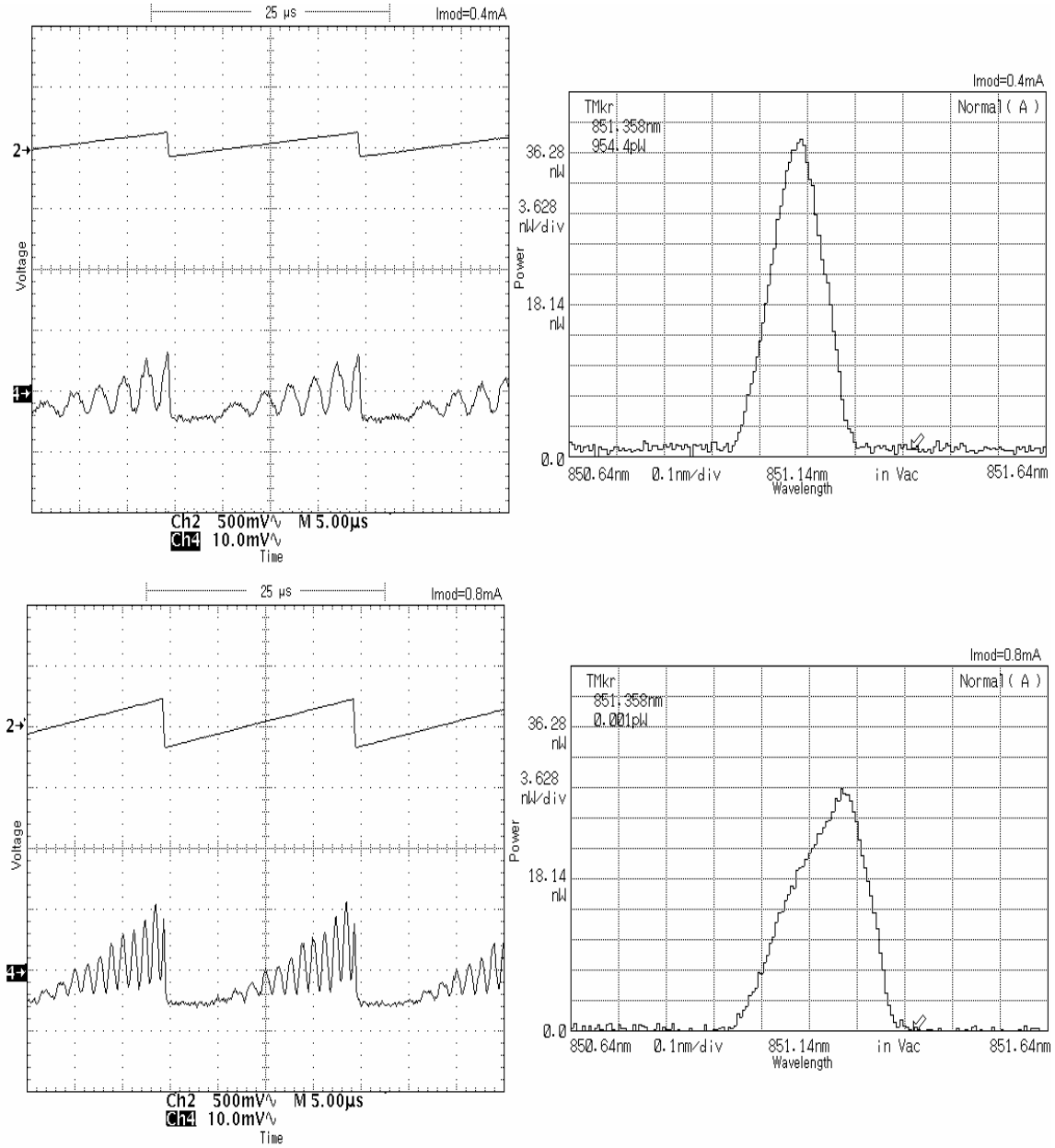

Fig. 34 Fringe pattern of FFPI sensor with SV3637 VCSEL at modulation currents of 0.4, 0.8, 1.2, and 1.6mA from top to bottom respectively. The modulation frequency is 50 kHz, the horizontal scale is 5µs/div, and the bias current is 1.8mA.

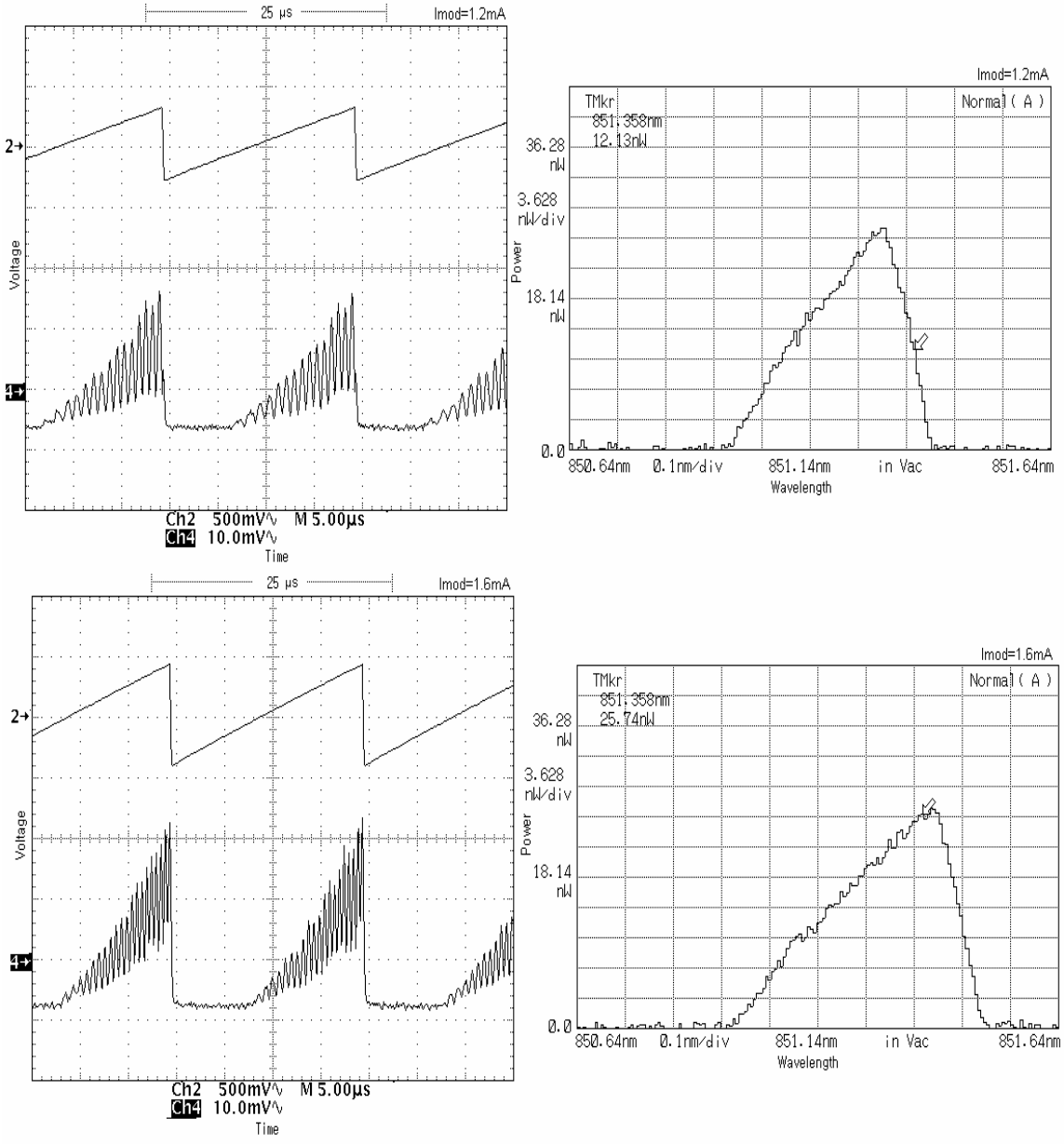

Fig. 34 (continued)

V. D Dependence of VCSEL frequency on drive current

The peak emission wavelength of VCSEL shifts as dc bias current increases. Fig. 35 shows the spectra of the VCSEL with dc bias current from 1.5mA to 4.5mA in increments of 0.3mA. Spectra for the case of saw-tooth modulation are shown in Fig.36, and fringe patterns are shown on Fig. 37 for each dc bias current. If the dc bias current is too high, the fringe pattern degrades, leading to poor FFPI sensor performance.

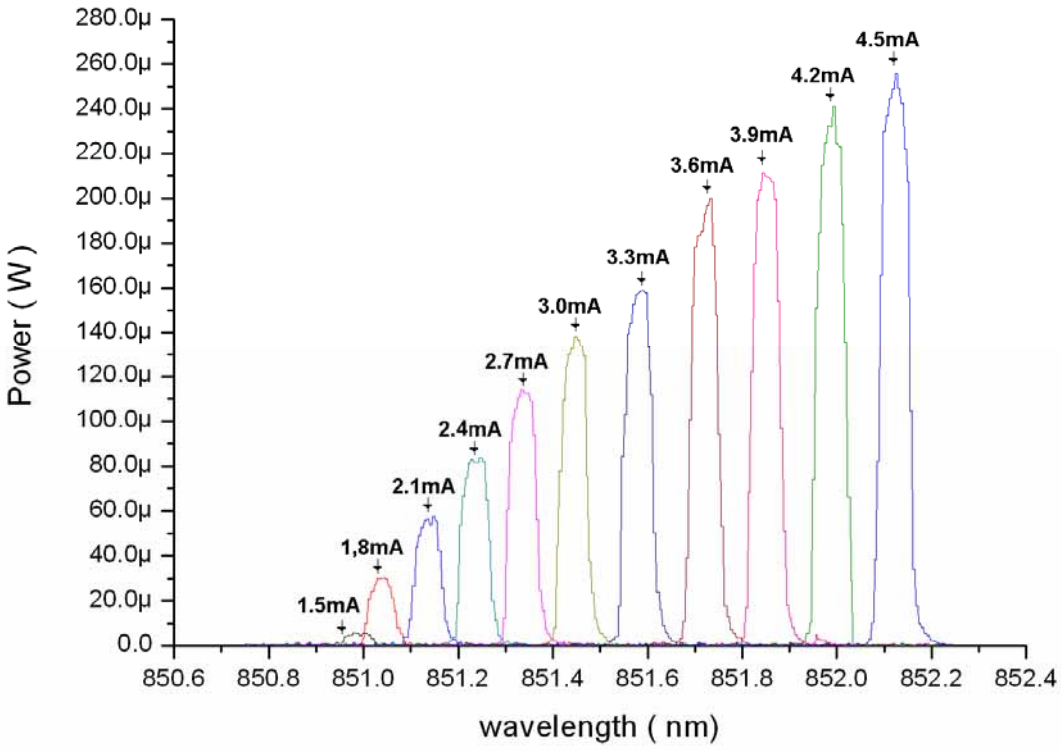

Fig. 35 Spectrum of dc biased SV3637 VCSEL.

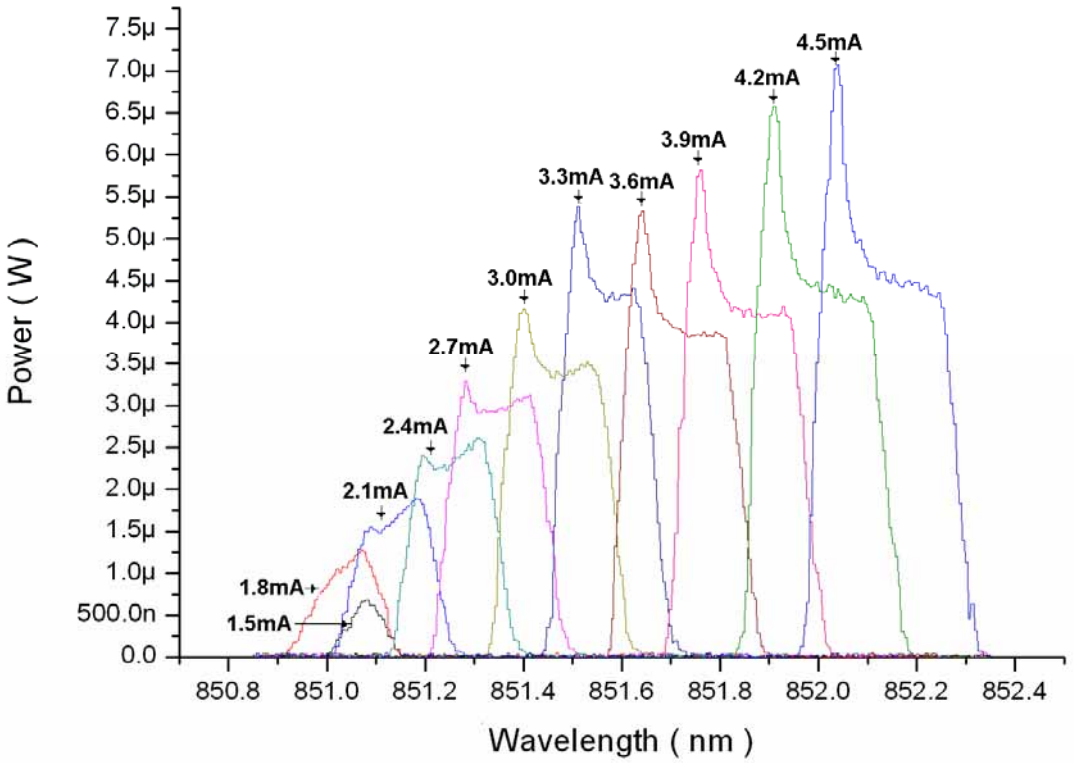

Fig. 36 Spectrum of SV3637 VCSEL with dc bias current when a saw-tooth modulation current is applied. Modulation frequency is 10kHz and modulation current is 0.6mA.

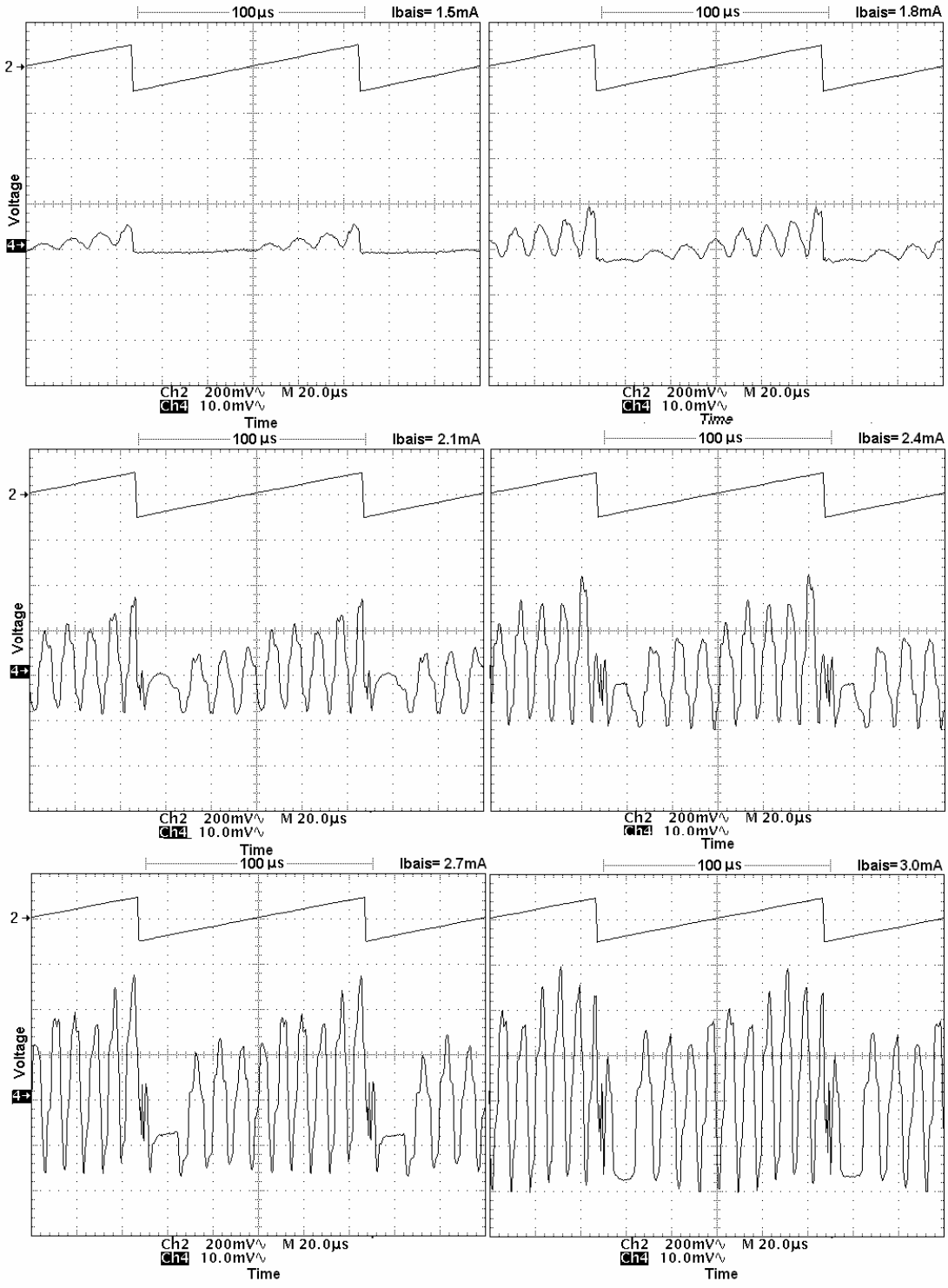

Fig. 37 Fringe pattern of FFPI on each saw-tooth wave form modulated VCSEL.

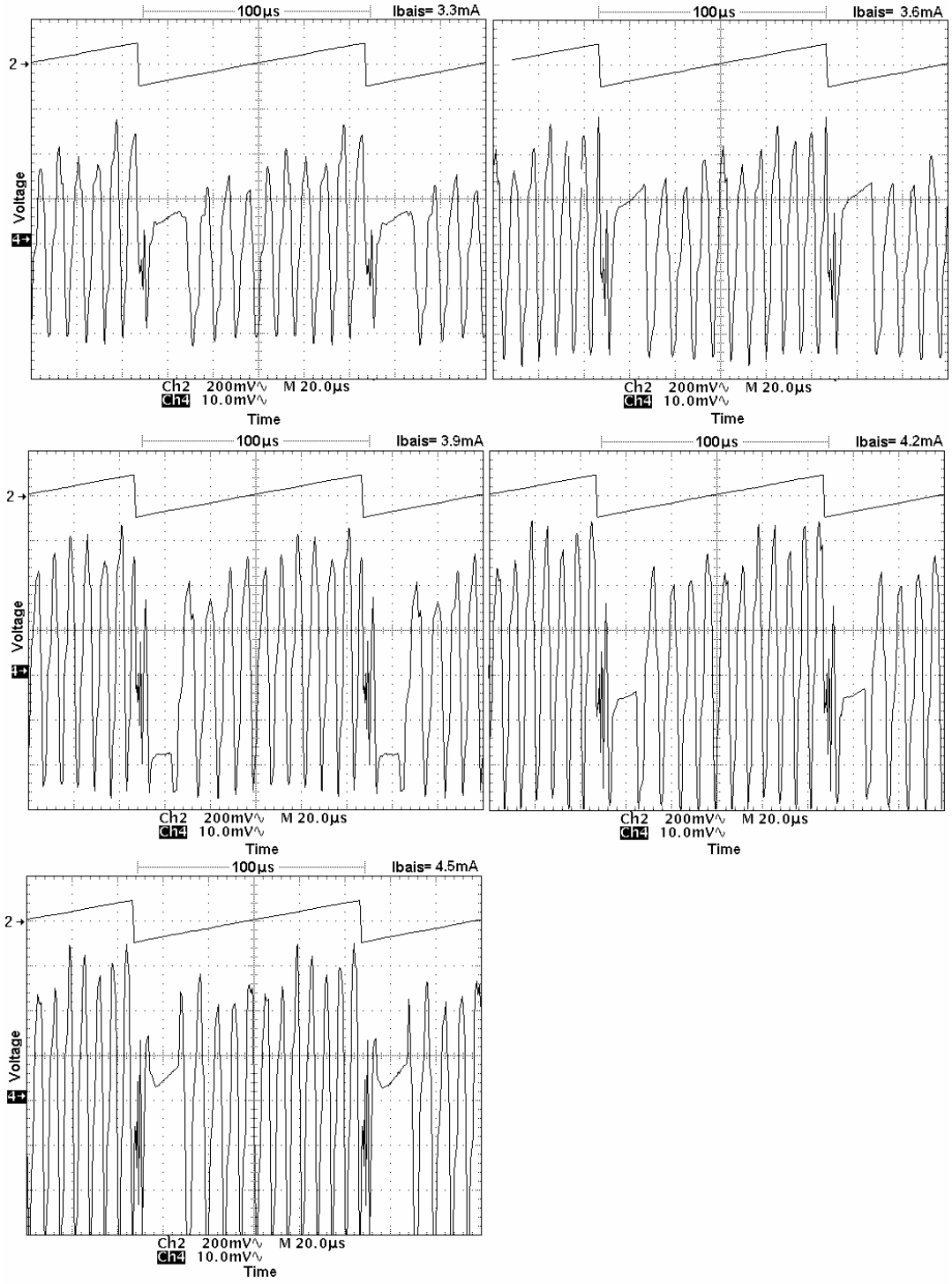

Fig. 37 (continued)

V. E Dependence of FFPI sensor fringe pattern on temperature

The experimental setup for the fringe pattern change as the FFPI is heated in an oven is illustrated in Fig. 38. As the temperature is increased in 1˚C increments from 131˚C to 140˚C, the fringe pattern moves to the right as shown in Fig. 39. The arrow indicates the peak of a particular fringe. The temperature increase required to displace the pattern one complete fringe is 3.5˚C. Thus, increasing the modulation current at a fixed bias current produces more fringes in given time regime.

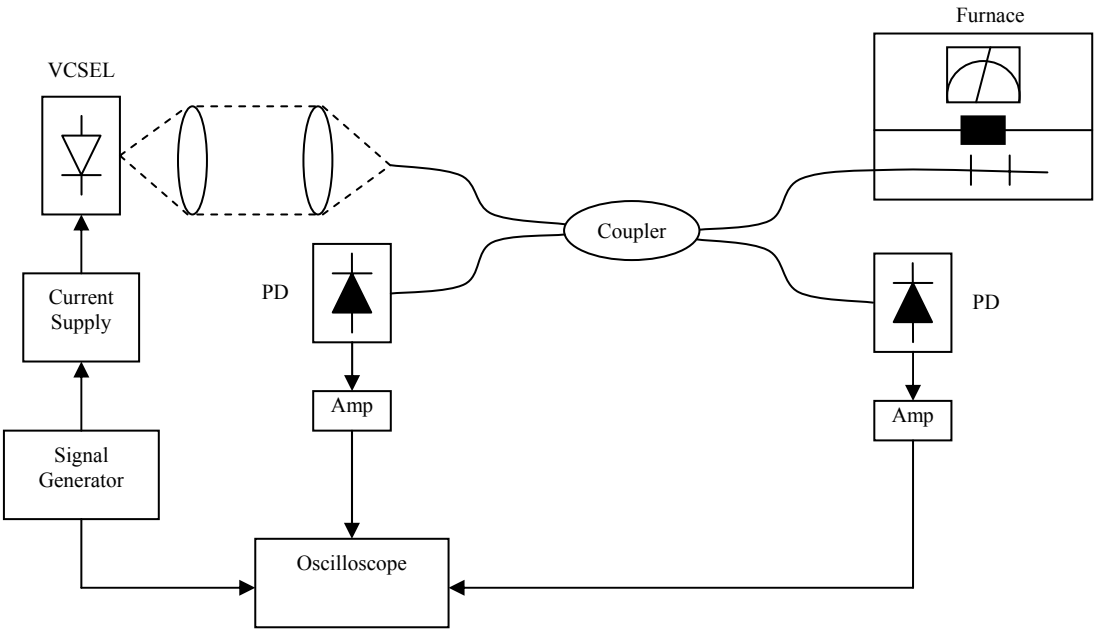

Fig. 38 Experiment setup for temperature dependence of fringe pattern.

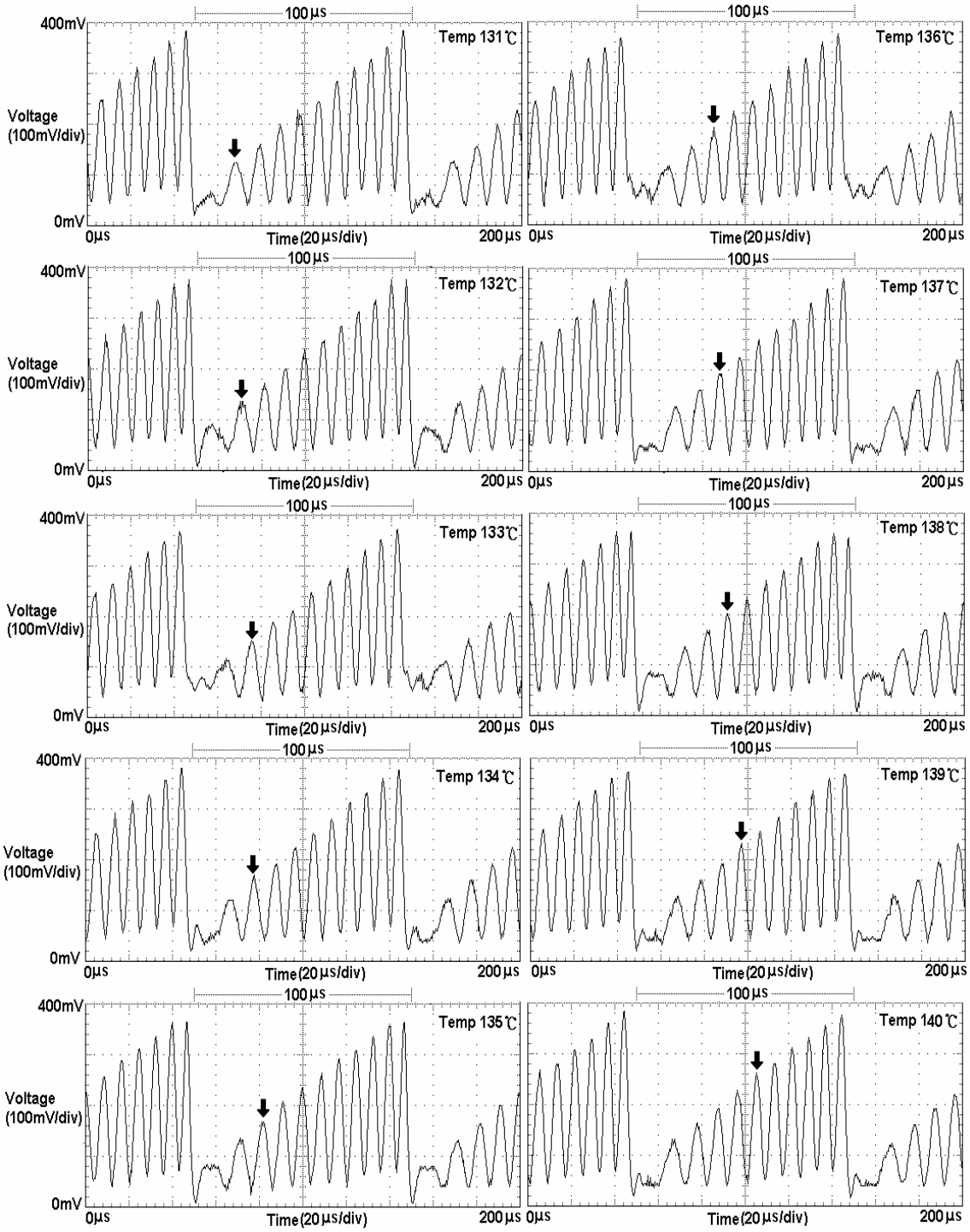

Fig. 39 Dependence of fringe pattern on temperature when the sensor is monitored with a 0.85µm VCSEL with temperature range of 131˚C to 140˚C.

CHAPTER VI

EXPERIMENTAL INVESTIGATIONS OF AN FFPI SENSOR MONITORED WITH A 1300nm EDGE EMITTING LASER

For comparison with the VCSEL results of chapter V, a 1.3μm DFB laser was used to monitor an FFPI sensor with the setup of Fig. 40. This setup uses SMF-28 fiber, which is single mode at a wavelength of 1.3μm. The fiber end is terminated so that no back reflection is produced.

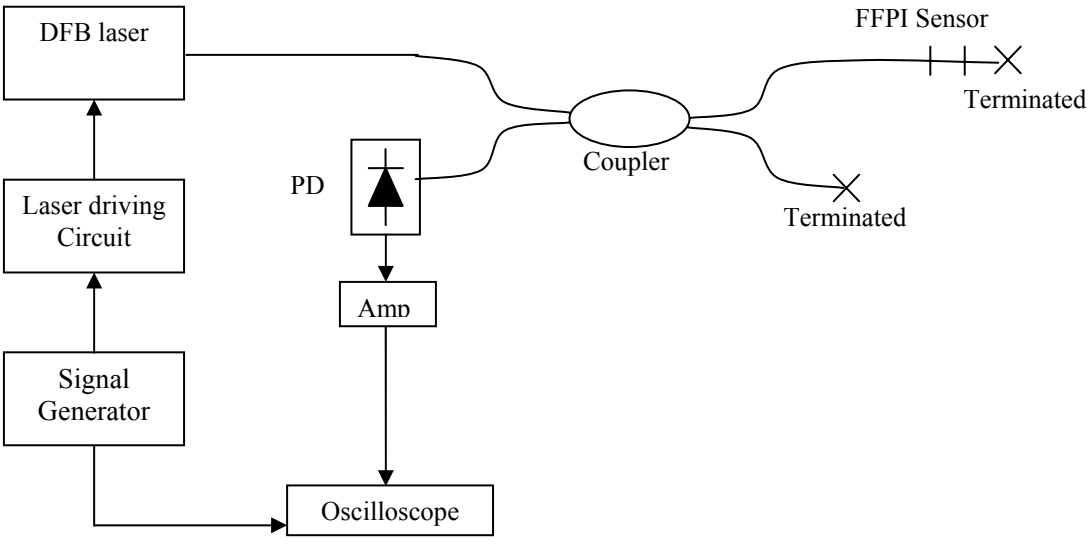

Fig .40 Experiment setup with 1.3μm DFB laser as light source.

Results are shown in Figs. 41, 42 and 43 for various bias currents, modulation currents, and modulation frequencies. In each cases, a square, triangular, and saw-tooth modulating wave form is applied. The cavity length is 12mm, same as in the 850nm experiment described previously.

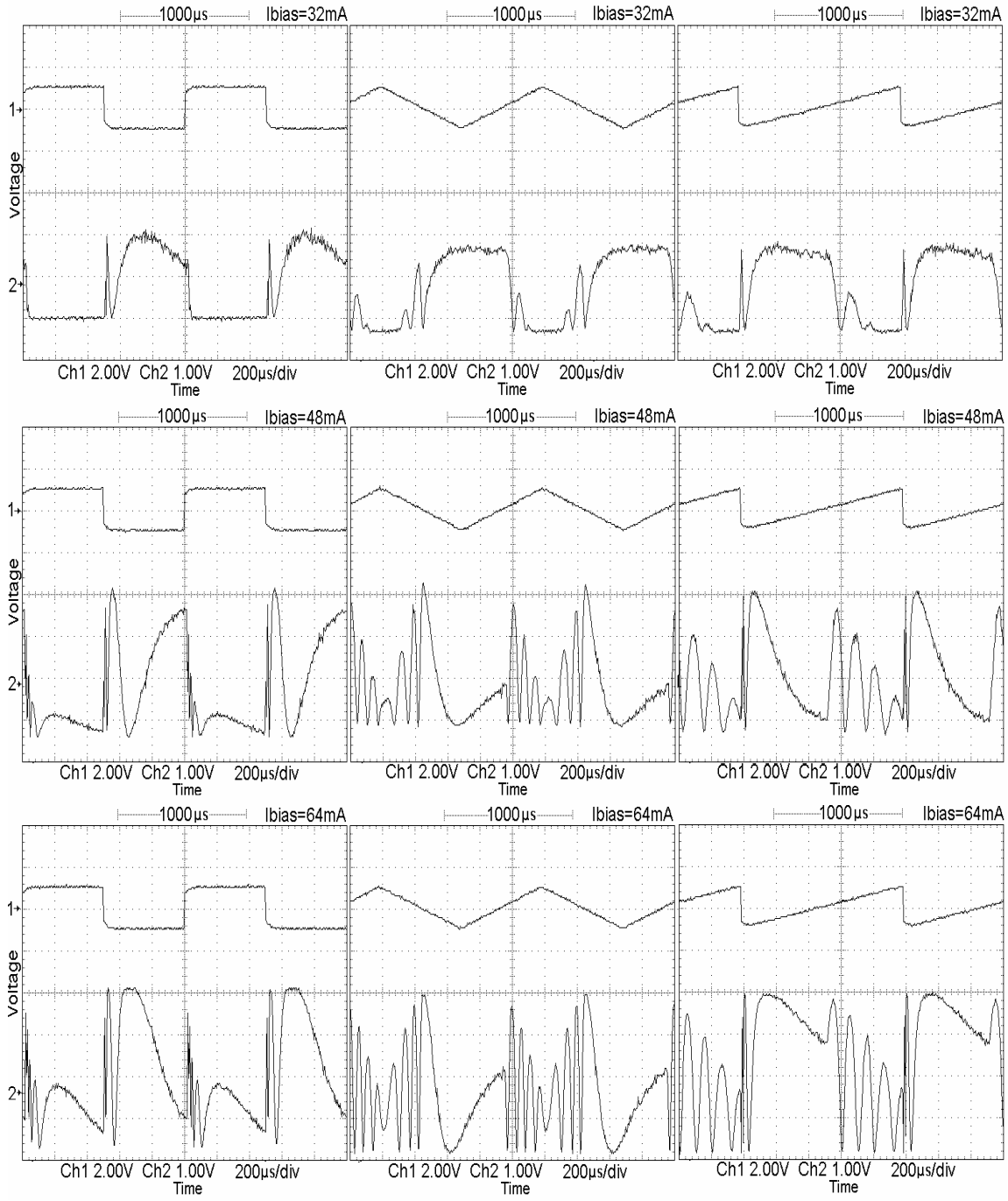

Fig. 41 Temporal dependence of bias current and sensor output power using a DFB laser light source emitting at 1300nm. The first row traces are for bias current of 32mA, the second row traces are for 48mA, and last row traces are for 64mA. In each case the modulation depth is 8mA, the horizontal scale is 200µs/div, and the modulation frequency is 1 kHz.

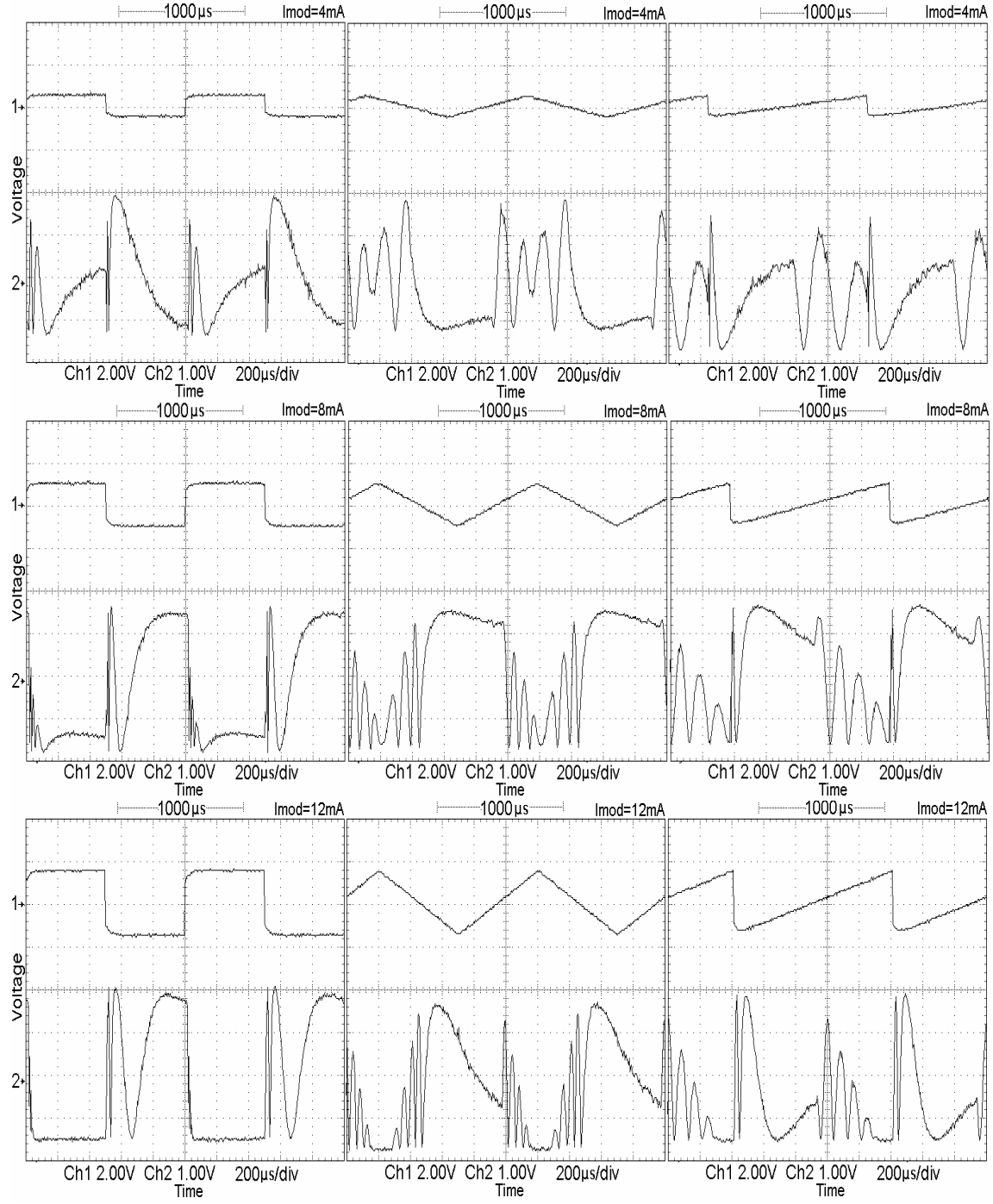

Fig. 42 Temporal dependence of modulation current and sensor output power using a DFB laser light source emitting at 1300nm. The first row traces are for modulation current of 4mA, the second row traces are for 8mA, and last row traces are for 12mA. In each case the bias current is 48mA, the horizontal scale is 200µs/div, and the modulation frequency is 1kHz.

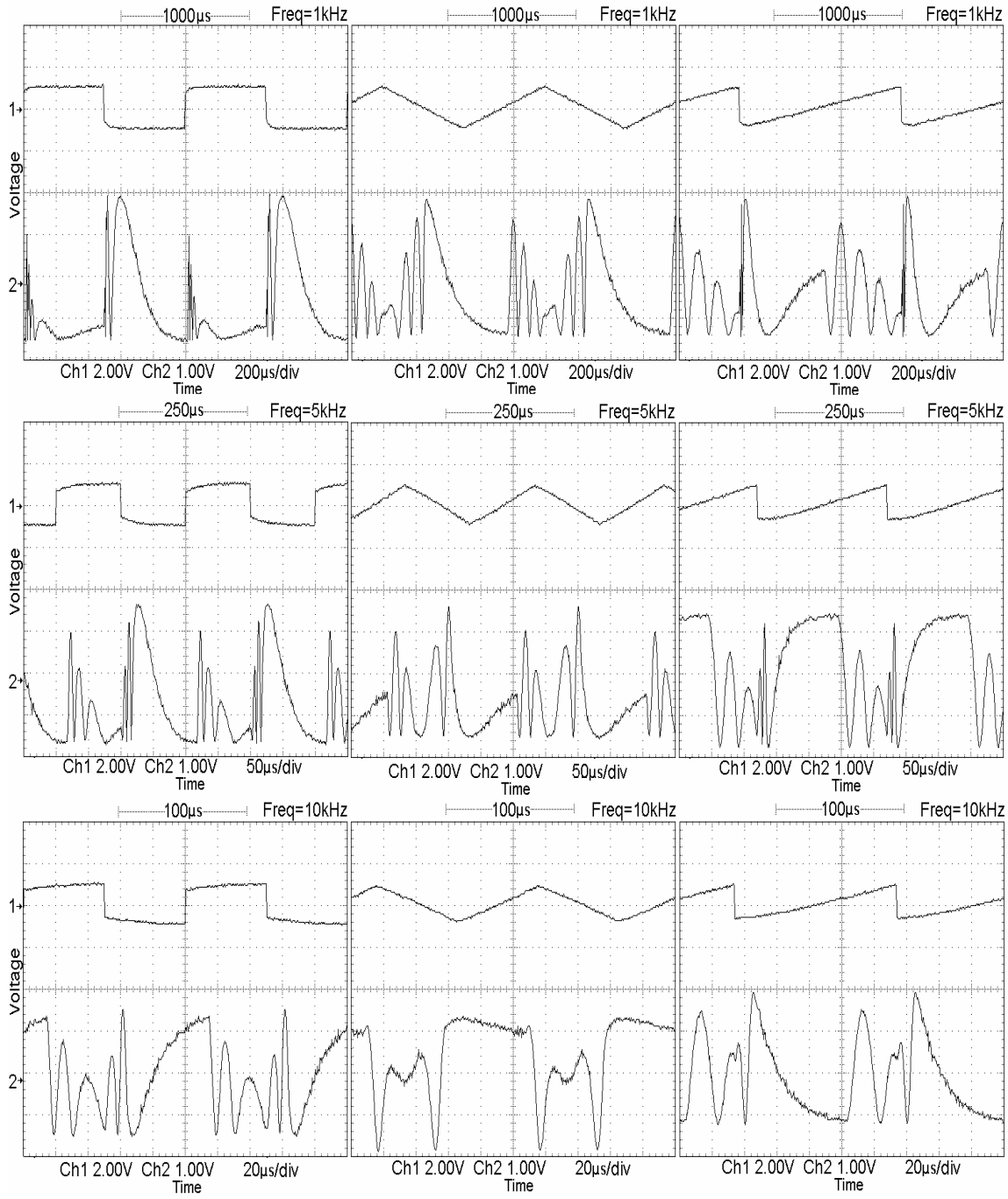

Fig. 43 Temporal dependence of modulation frequency and sensor output power using a DFB laser light source emitting at 1300nm. The first row traces are for modulation frequency of 1kHz, the second row traces are for 5kHz, and last row traces are for 10kHz with the horizontal scale of 200µs/div, 50µs/div, and 20µs/div respectively.. In each case the bias current is 48mA, and the modulation current is 8mA.

CHAPTER VII

DISCUSSION AND ANALYSIS OF RESULTS

The data presented in Chapter V can be analyzed to obtain useful information on both the laser and on the single mode fiber used in the FFPI sensor.

From the data of Fig. 35, it is evident that the peak wavelength of the VCSEL emission λ changes from 851.04 nm at a bias current I of 1.8 mA to 852.12 nm at I = 4.5 mA. Thus, the current tuning factor for this laser is

$$\frac{d\lambda}{dI} = 0.40 \text{nm} / \text{mA} \tag{15}$$

From this result, the dependence of VCSEL frequency ν on current can be calculated from the expression

$$\frac{d\nu}{dI} = \frac{d\lambda}{dI}\frac{d\nu}{d\lambda} \tag{16}$$

From the equation $\lambda\nu = c$, with c the free-space speed of light, it follows that

$$\frac{d\nu}{d\lambda} = -\frac{c}{\lambda^2} \tag{17}$$

and from eq. (16) and eq. (17),

$$\frac{d\nu}{dI} = -\frac{c}{\lambda^2}\frac{d\lambda}{dI} \tag{18}$$

Using the values c = 3.00 x 10^8 m/s and λ = 851.58 nm, it follows from eqs. (15) and (18) that

$$\frac{d\nu}{dI} = -165\text{GHz/mA} \tag{19}$$

Another way to determine the dependence of laser frequency on drive current is to count the fringes produced by a time-varying drive current, and relate the number of fringes to the frequency change. The free spectral range of the FFPI $\Delta\nu_{FSR}$ is the laser frequency change for which $\Delta\phi = 2\pi$, and it follows from eq. (7) that

$$\Delta\nu_{FSR} = \frac{c}{2n_g L} \tag{20}$$

with n_g the group refractive index of the fiber mode. Using the parameters n_g = 1.47 and L = 1.2 cm, it follows from eq. (20) that

$$\Delta\nu_{FSR} = 8.5 \text{ x } 10^9 \text{ Hz} = 8.5 \text{ GHz} \tag{21}$$

As an example of the frequency shift calculation, it is determined from the data of Fig. 21 for VCSEL SV3639 at a bias current of 1.8 mA modulated with a sawtooth waveform at a frequency of 10 kHz that the tuning rate is 19.3 fringes per mA. From eq. (21), this corresponds to a tuning rate of

$$\frac{d\nu}{dI} = -164\text{GHz/mA} \tag{22}$$

Thus, the frequency tuning from the modulation/fringe counting measurement gives almost the same result as the dc bias/spectral shift measurement of eq. (19), indicating

that the laser is near thermal equilibrium at the 10 kHz modulation frequency. From the data of Fig. 30, it is seen that the number of fringes decreases by about 20% when the modulation frequency is increased from 10 kHz to 100 kHz, so that at the higher modulation frequency thermal equilibrium is not achieved throughout a modulation cycle.

The temperature increase responsible for tuning the laser can also be estimated. From the expression

$$\frac{d\nu}{dT} = \frac{d\lambda}{dT}\frac{d\nu}{d\lambda} \tag{23}$$

and eq. (17), it follows that

$$\frac{d\nu}{dT} = -\frac{c}{\lambda^2}\frac{d\lambda}{dT} \tag{24}$$

Using the value of the wavelength temperature coefficient

$$\frac{d\lambda}{dT} = 0.06\text{nm}/°\text{C} \tag{25}$$

given by the VCSEL manufacturer, it follows from eq. (24) that

$$\frac{d\nu}{dT} = -24.8\text{GHz}/°\text{C} \tag{26}$$

It follows from this result and eq. (19) that

$$\frac{dT}{dI} = 6.65°\text{C}/\text{mA} \tag{27}$$

The dependence of optical path length of the FFPI cavity nL on temperature T can be calculated using eq. (7), from which it follows that

$$\frac{d\phi}{dT} = \frac{\phi}{nL}\frac{d(nL)}{dT} \tag{28}$$

Using the parameters n = 1.458 and L = 1.2 cm, it follows from eq. (7) that

$$\phi = 4.11 \text{ x } 10^4 \text{ x } 2\pi \quad \text{rad} \tag{29}$$

From the observation (Fig. 39) that a change in the FFPI temperature $\Delta T = 3.5^{\circ}C$ tunes the optical signal through one fringe, corresponding to $\phi = 2\pi$ rad, the temperature tuning coefficient for the optical path length of the interferometer is

$$\frac{1}{nL}\frac{d(nL)}{dT} = 6.95 \text{x} 10^{-6} / {}^{\circ}C \tag{30}$$

This is slightly (3.5%) less than a value of $7.2 \text{ x } 10^{-6}/^{\circ}C$ measured at 1300 nm in a single mode Corning fiber [6].

CHAPTER VIII

CONCLUSIONS

The use of 850nm vertical cavity surface emitting lasers (VCSELs) were investigated for monitoring an interferometric fiber optic sensor, and the results were compared with those obtained with a conventional distributed feedback (DFB)laser. In both cases, fiber Fabry Perot interferometer (FFPI) sensors with 85.5nm thick internal dielectric mirrors and a 12mm cavity length were monitored with the laser system.

With a VCSEL as the light source, mode- hopping, which is commonly observed with other lasers due to back reflection of light, is avoided by using angle polished fiber ends, tilting coupling lenses, using anti-reflection coated lenses, and tilting the photo diode. Even with these precautions, a considerable amount of back reflected light was coupled into the VCSEL from the FFPI sensor. Despite the fact that no Faraday isolator was used, regular fringe patterns with over 20 fringes were observed at the highest modulation current amplitudes.

The spectral characteristics of the laser and the fringe patterns of reflected light from the FFPI sensor were investigated over a range of dc bias currents from 1.2mA to 2.2mA and peak-to-peak modulation current amplitudes from 0.24mA to 1.08mA to determine combinations which gave single mode laser operation and high quality fringe patterns.

The laser tuning rate with drive current was determined to be -165 GHz/mA from measurements of the shift in the spectral peak of the laser output as a function of dc bias

current. This was in good agreement with an independent measurement of the same parameter obtained by counting fringes from the FFPI sensor as the laser was modulated at a frequency of 10 kHz. From this, it was concluded that the heating responsible for spectral tuning of the laser was an adiabatic process at that modulation frequency. The tuning rate was found to decrease by about 20% at 100 kHz modulation frequency, so thermal equilibrium was not reached at that modulation frequency.

From the VCSEL manufacturer's data on wavelength temperature coefficient, together with the measured spectral tuning as a function of drive current, it was determined that the temperature change in the laser cavity was 6.65 ºC/mA.

By heating the FFPI sensor, it was determined that a 3.5 ºC temperature change is required to shift the reflected light pattern by one fringe. From this data, it was deduced that the fractional change in optical path length with temperature in the 850 nm single mode fiber was 6.95×10^{-6} ºC, in good agreement with earlier measurements on a 1300 nm fiber.

For comparison, similar experiments were carried out using a 1300 nm distributed feedback (DFB) laser and an FFPI sensor made with a 1300 nm single mode fiber. The DFB/FFPI combination required much higher dc bias current and current modulation amplitude to produce a given number of fringes. The fringe patterns were also much less regular than the VCSEL/850 nm FFPI combination. This observation, plus the fact that VCSELs are much less expensive than DFB lasers and don't require Faraday isolators, makes the vertical cavity laser an attractive alternative for monitoring interferometric sensors such as the FFPI.

CHAPTER IX

RECOMMENDATIONS

More work is needed to understand the relative immunity of VCSELs to optical feedback. Controlled tests of the spectra and FFPI sensor response as a function of feedback level and distance to the source of feedback would be useful. Experiments in which a Faraday isolator was used to eliminate feedback would also be desirable.

Efforts should be made to apply the VCSEL to practical sensors for pressure, temperature, strain, and other parameters.

Since single mode 1300 nm VCSELs are now available, studies similar to those reported above should be made of the spectral and modulation characteristics of these lasers.

REFERENCES

[1] T. G. Giallorenzi, J. A Bucaro, A. Dandridge, G. H. Siegel, Jr., J. H. Cole, S.C. Rashleigh, and R. G. Priest, "Optical fiber sensor technology," *IEEE Journal of Quantum Electronics*, vol. QE-18, no. 4, pp. 626-664, Apr. 1982.

[2] T. G. Giallorenzi, J. A Bucaro, A. Dandridge, and J. H. Cole, "Optical fiber sensors challenge the competition," *IEEE Spectrum*, vol. 23, no. 9, pp. 44-49, 1986.

[3] R. A. Bergh, H. C. Lefevre, and H. J. Shaw, "An overview of fiber optics gyroscopes," *Journal of Lightwave Technology*, vol. 2, no. 2, pp. 91-96, 1984.

[4] J. P. Dakin, C. A. Wade, and M. Henning, "Novel optical fibre hydrophone arrays using a single laser source and detector," *Electronics Lett.*, vol. 20, pp 53-54, 1984

[5] E. L. Green, G. E. Holmberg, J. C. Gremillion, and F. C. Allard, "Remote passive phase sensor," in *Proc. Third Int. Conf. on Optical Fiber Sensors*, San Francisco, CA., p. 130, Feb. 1985.

[6] C. E. Lee, and H. F. Taylor, "Interferometric optical fibre sensors using internal mirrors," *Electronics Lett*., vol. 24, no. 4, pp. 193-194, Feb. 1998.

[7] C. E. Lee, R. A. Atkins, and H. F. Taylor, "Performance of a fiber optic temperature sensor from -200 to 1050˚C," *Opt Lett.,* vol. 13, pp. 1038-1040, Nov. 1988.

[8] C. E. Lee, H. F. Taylor, A. M. Marcus, and E. Udd, "Optical-fiber Fabry-Perot embedded sensor," *Opt. Lett*., vol. 14, pp. 1225-1227, Nov. 1, 1989.

[9] J. J. Alcoz, C. E. Lee, and H. F. Taylor, "Embedded fiber-optic Fabry-Perot ultrasound sensor," *IEEE Trans. Ultrason., Ferroelec., Freq. Contr.,* vol. 37, pp. 302-306, Jul. 1990.

[10] J. F. Dorighi, S. Krishnaswamy, and J. D. Achenbach, "Stabilization of an embedded fiber optic Fabry-Perot sensor for ultrasound detection," *IEEE Trans. Ultrason., Ferroelec., Freq. Contr.,* vol. 42, pp. 820-824 Jul. 1995.

[11] C. E. Lee, W. N. Gibler, R. A. Atkins, and H. F. Taylor, "In-line fiber Fabry-Perot interferometer with high reflectance internal mirrors," *Journal of Lightwave Technology,* vol. 10, pp. 1376-1379, Oct. 1992.

[12] C. E. Lee and H. F. Taylor, "Fiber–optic Fabry-Perot temperature sensor using low-coherence light source," *Journal of Lightwave Technology,* vol. 9, pp. 129-134, Jan. 1991.

[13] H. S. Chio, H. F. Taylor and C. E. Lee, "High performance fiber-opic temperature sensor using low-coherence interferometry," *Opt. Lett.*, vol. 22, no. 23, pp. 1814-1816, 1997.

[14] Y. Park, "Development and testing of fiber optic current transducer with digital signal processing," Ph.D. dissertation, Texas A&M University, College Station, May 1995.

[15] R. Sadkowski, C. E. Lee, and H. F. Taylor, "Multiplexed interferometric fiber-optic sensors with digital signal processing," *Appl. Opt.,* vol. 34, no. 25, pp 5861-5866, Sept 1995.

[16] R. A. Atkins, J. H. Gardner, W. N. Gibler, C. E. Lee, M. D. Oakland, M. O. Spears, V. P. Swenson, H. F. Taylor, J. J. McCoy, and G. Beshouri, "Fiber-optic pressure sensors for internal combustion engines," *Appl. Opt.,* vol. 33, pp 1315-1320, 1994.

[17] C. E. Lee, and H. F. Taylor, "A fiber optic pressure sensor for internal combustion engines," *Sensors,* vol. 15, no. 3, pp 193-195, 1998.

[18] T. Bae, "Spark-plug mounted fiber optic sensor for measuring in-cylinder pressure in engines," M.S. thesis, Texas A&M University, College Station, Dec. 2001.

[19] W. Lee, "Railroad bridge monitoring systems with fiber optic sensors," Ph.D. dissertation, Texas A&M University, College Station, Aug.1998.

VITA

Kyung-Woo Lee was born in Seoul, Korea on September 7, 1972. He received his B. S. degree in radio science engineering from Hanyang University, Seoul, Korea in February 1998. During March 1998 to June 1998, he worked as discipline researcher in Electronics and Telecommunication Research Institute. He received M.S. degree in electrical engineering from Texas A&M University, College Station in December 2000. He began working on his Ph.D. in January 2001, and in August 2005, received his Ph.D. advised by Dr. Henry F. Taylor. His major interests include fiber optic sensors, fiber optic communications, passive optical network (PON) on fiber to the home (FTTH), optical filters, and WDM systems.

He can be reached at following address:

Kyung-Woo Lee

Guseong-eup Bojung-ri Yongin-si

Donga Solecity 130-1802

Gyeonggi-do, 449-940 Korea

kyungwoo@ee.tamu.edu